

~~CONFIDENTIAL~~

Copy 293
RM E57F13

OCT 9 - 1957
7259

0143942



TECH LIBRARY KAFB, NM

NACA RM E57F13

7023

NACA

RESEARCH MEMORANDUM

INTERNAL PERFORMANCE OF SEVERAL DIVERGENT -SHROUD

EJECTOR NOZZLES WITH HIGH DIVERGENCE ANGLES

By Arthur M. Trout, S. Stephen Papell, and John H. Povolny

Lewis Flight Propulsion Laboratory
Cleveland, Ohio

Classification cancelled (or changed to Unclassified)

By Authority of NASA Tech Rep Announcement #33
(OFFICER AUTHORIZED TO CHANGE)

By 24 Nov 60

..... NK

GRADE OF OFFICER MAKING CHANGE)

..... 13 Feb 61

DATE

CLASSIFIED DOCUMENT

This material contains information affecting the National Defense of the United States within the meaning of the espionage laws, Title 18, U.S.C., Secs. 793 and 794, the transmission or revelation of which in any manner to an unauthorized person is prohibited by law.

NATIONAL ADVISORY COMMITTEE FOR AERONAUTICS

WASHINGTON

October 2, 1957

~~CONFIDENTIAL~~



NATIONAL ADVISORY COMMITTEE FOR AERONAUTICS

RESEARCH MEMORANDUMINTERNAL PERFORMANCE OF SEVERAL DIVERGENT-SHROUD EJECTOR
NOZZLES WITH HIGH DIVERGENCE ANGLES

By Arthur M. Trout, S. Stephen Papell, and John H. Povolny

SUMMARY

Nine divergent-shroud ejector configurations were investigated to determine the effect of shroud divergence angle on ejector internal performance. Unheated dry air was used for both the primary and secondary flows.

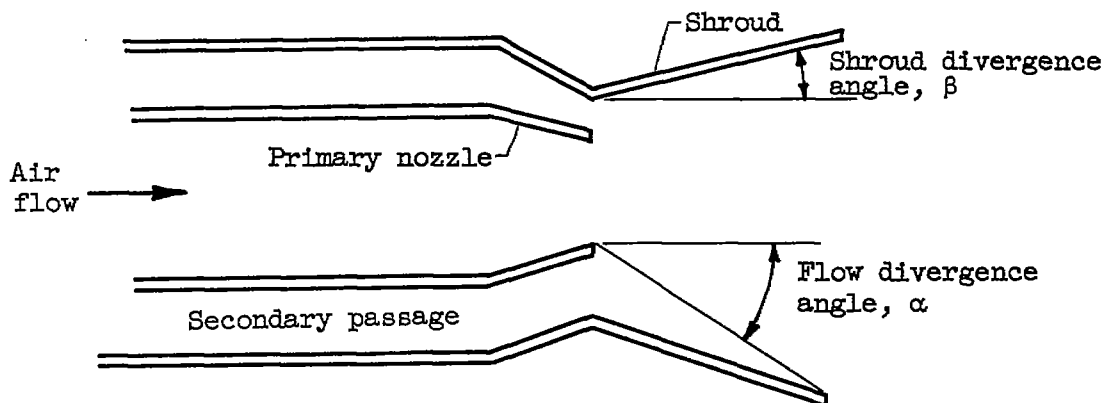
The decrease in the design-point thrust coefficient with increasing flow divergence angle (angle measured from primary exit to shroud exit) followed very closely a simple relation involving the cosine of the angle. This indicates that design-point thrust performance for divergent-shroud ejectors can be predicted with reasonable accuracy within the range investigated. The decrease in design-point thrust coefficient due to increasing the flow divergence angle from 12° to 30° (half-angles) was approximately 6 percent. Ejector air-handling characteristics and the primary-nozzle flow coefficient were not significantly affected by change in shroud divergence angle.

INTRODUCTION

The advent of supersonic flight has increased the available exhaust-nozzle pressure ratio of turbojet-powered aircraft to such an extent that the convergent nozzles used in the subsonic regime become prohibitively inefficient. Reference 1 shows that divergent-shroud ejector nozzles can be used to expand the engine exhaust gases efficiently at high pressure ratios and at the same time provide cooling air for the engine, the afterburner, and the nozzle by the flow of secondary air.

The various configurations of reference 1 covered a range of design pressure ratios but were limited to relatively low shroud divergence angles. The shroud divergence angles investigated varied from 3° to 12° (see sketch).



~~CONFIDENTIAL~~

Appreciable savings in structural weight and shroud cooling-air requirements can be made if the shroud divergence angle β is increased for any given design, thus shortening the ejector shroud. It is to be expected, however, that, as the divergence angle is increased, the losses due to nonaxial velocity components at the nozzle exit will also increase, just as is shown to be the case for conical convergent-divergent nozzles in reference 2.

The investigation reported hereinafter extends three representative ejector designs of reference 1 to shroud angles β of 15° , 20° , and 25° in order to determine the effect of shroud angle on ejector nozzle performance. The three groups of ejectors have design pressure ratios of approximately 6.5, 12, and 25; and the test conditions covered a range of primary-nozzle pressure ratios from about 1.8 to a value beyond the design point for each configuration.

Secondary weight flow was varied from zero to a value which made the secondary total pressure nearly equal to the primary total pressure. This resulted in secondary weight flows of from zero to about 16 percent of the primary airflow. The tests were conducted with dry air at approximately 60° F for both the primary and secondary flows. Unpublished NACA data indicate that the performance of a given ejector nozzle is essentially the same when hot exhaust gas instead of unheated air is used for the primary stream.

APPARATUS AND INSTRUMENTATION

Test Facility

The ejector models were installed in a 6-foot-diameter test chamber shown photographically in figure 1. Figure 2 is a diagrammatic sketch of the test facility. The ejector models and the air-supply pipes were freely suspended in the chamber by four flexure rods. The resultant axial force acting on the ejector installation during the tests was transmitted through a flexure-plate-supported bell crank and linkage to

~~CONFIDENTIAL~~

a calibrated null-type pneumatic force-measuring cell. Pressure gradients on the diffuser section of the primary-air inlet pipe were prevented by a vent line which connected the annular region between the labyrinth seals to the test chamber. This minimized the pressure drop and the airflow through the second seal. Secondary air was supplied through a 6-inch flexible rubber hose which was connected perpendicularly to the ejector axis so that no axial forces could be transmitted to the rig when the hose was pressurized. The secondary-air-supply pipe included an orifice assembly for measuring secondary airflow.

Ejector Models

The geometries of the nine ejector models investigated and the three low-shroud-angle counterparts from reference 1 are given in table I. The three groups of ejectors had exit diameter ratios of about 1.24, 1.46, and 1.82, which correspond to design pressure ratios of 6.5, 12, and 25, respectively.

The minimum area of the shroud (the point at which D_g is measured) was arbitrarily placed in the plane of the primary-nozzle exit for this investigation (see sketch, table I). Practical ejector design considerations may often make it necessary or desirable to move this shroud minimum area slightly downstream of the plane of the primary-nozzle exit and to contour this region of the shroud. This would not be expected to have significant effect on the ejector performance as long as the primary jet does not expand to an area greater than the shroud minimum area at any point upstream of the minimum shroud area.

Configurations 1 to 6 were run with a primary nozzle of 8.30-inch exit diameter. This relatively large nozzle passed sufficient air, however, to cause excessive pressure losses in the exhaust system, thereby limiting the maximum primary-nozzle pressure ratio for these six configurations to values under 16. In order to reach design pressure ratio for configurations 7, 8, and 9, the models were scaled down for use with a 6.50-inch-diameter primary nozzle. (The primary-nozzle convergence angle was 8° for both primary nozzles.)

Instrumentation

Pressure measurements were made at the various stations indicated in figures 2 and 3. The type of instrumentation at each location is given in table II. The total temperature of the primary air was measured by means of two iron-constantan thermocouples several feet upstream of station 1. The secondary-air temperature, measured by a single thermocouple in the secondary-air-supply pipe, was the same as that for the primary stream inasmuch as both were supplied from the same header.

PROCEDURE

The performance of each ejector configuration was obtained as follows: (1) Pressurized air (40 lb/sq in. gage) from the laboratory supply system was throttled to a reduced pressure of about 45 inches of mercury absolute upstream of station 1 (fig. 2). (This inlet pressure gave nearly the maximum primary pressure ratios obtainable with this facility.) (2) The test-chamber exhaust line was fully opened to the exhaust system (26 in. Hg, vacuum), resulting in a maximum primary-nozzle pressure ratio of about 16 to 18 for the 8.30-inch-diameter primary nozzle and 28 to 30 for the 6.50-inch-diameter primary nozzle. (3) The ejector performance for zero secondary airflow was then obtained by maintaining a constant header pressure upstream of the inlet throttling valve, while the exhaust pressure was raised in steps by closing the exhaust valves downstream of the test chamber until a primary pressure ratio of slightly less than 2 was obtained for each configuration. (4) The exhaust pressure was then reduced again to a minimum value, and secondary airflow was introduced through a throttling valve downstream of the secondary-air measuring orifice. For each setting of secondary airflow, the ejector performance over a complete range of primary-nozzle pressure ratios was obtained as in step (3). The secondary weight-flow ratio was increased in three or four arbitrary steps, with the maximum value being obtained when the secondary total pressure was equal to the primary total pressure. This resulted in secondary weight-flow ratios of approximately 10 percent for configurations 1, 2, and 3 and 16 percent for the other configurations. The ejector weight-flow ratio remained constant for any given setting of the secondary-air throttling valve even though at low primary-nozzle pressure ratios both the secondary passage and the primary nozzle were unchoked. This was due to the fact that both primary and secondary flows were supplied from a common source and the throttling valves were choked at all times.

Preliminary tests indicated no significant difference in total-pressure measurements between stations s and s' (fig. 3). There were slight variations, however, in the circumferential total-pressure distribution at station s' for high secondary weight flows. Therefore, the secondary pressure measurements at station s' rather than at station s were used in the calculations.

Symbols are defined in appendix A, and the methods of calculation are given in appendix B.

RESULTS AND DISCUSSION

Performance of Primary Nozzles

The thrust and flow (or discharge) coefficients for both of the primary nozzles which were used with the ejector models are shown in

figure 4 for a range of pressure ratios. The thrust coefficient (fig. 4(a)) is defined as the ratio of measured jet thrust to ideal (one-dimensional) jet thrust for the measured weight flow expanded isentropically through the same (measured) pressure ratio. The flow coefficient (fig. 4(b)) is the ratio of measured corrected weight flow to ideal (one-dimensional) corrected weight flow for the same pressure ratio.

The thrust-coefficient level for the primary nozzles is about 1 to $1\frac{1}{2}$ percent higher than that indicated by previously published data for convergent nozzles (refs. 1 and 3 to 8). However, because of the extensive calibrations and checks made on the test rig, the relative thrust values reported herein are believed reliable. Error analysis of measurements showed a probable mean error of about ± 1 percent for thrust coefficient.

The flow-coefficient data are in good agreement with other data for similar nozzles (refs. 5 to 8).

Ejector Performance

Performance data for ejector configurations. - The performance of each of the nine ejector-nozzle configurations is presented in figures 5 to 13. For each ejector the following data plots are shown:

- (1) Ratio of ejector thrust to ideal primary-nozzle thrust F_{ej}/F_{ip}
- (2) Ejector thrust coefficient $F_{ej}/(F_{ip} + F_{is})$
- (3) Ejector total-pressure ratio $(P_s/P_p)_{ej}$
- (4) Primary-nozzle flow coefficient $\left(\frac{w_{a,2}\sqrt{\theta_p}}{A_p\delta_p}\right) / \left(\frac{w\sqrt{\theta}}{A\delta}\right)_i$

Each of these quantities is plotted against primary-nozzle pressure ratio for several constant values of secondary-to-primary corrected weight-flow ratio $(w_s/w_p)\sqrt{T_s/T_p}$. Secondary- and primary-air temperatures were the same for this investigation, but the use of the conventional generalized ejector performance parameter $(w_s/w_p)\sqrt{T_s/T_p}$ has been retained in the figures. Unpublished NACA data indicate that the weight flow correction factor $\sqrt{T_s/T_p}$ is sufficient to correlate ejector nozzle thrust and pumping characteristics when hot exhaust gas rather than unheated dry air is used for the primary jet.

The ratio of ejector jet thrust to ideal primary-nozzle thrust (isentropic one-dimensional expansion of the measured primary weight flow) is convenient in estimating the gross thrust of an engine of known thrust performance that is equipped with an ejector nozzle similar to

one of the model ejectors. For example, a typical use of this ratio would be as follows:

$$F_{ej} = \left(\frac{F_{ej}}{F_{ip}} \right) F \frac{F_p}{F_{ip}}$$

where F_{ej}/F_{ip} is obtained from the performance data for the desired pressure ratio and secondary weight-flow ratio, F is the known (convergent) primary-nozzle (or engine) thrust with no ejector, and F_p/F_{ip} is the primary-nozzle thrust coefficient for the desired pressure ratio from figure 4.

The ejector thrust coefficient is defined as the ratio of measured ejector thrust to the sum of the ideal (one-dimensional isentropic expansion) thrusts of both the primary and secondary streams using the measured values of airflow and pressure ratio. This coefficient is a measure of the efficiency with which the ejector nozzle converts the combined available energy of primary and secondary streams to useful thrust. The secondary weight flow for optimum gross ejector thrust is readily seen from such a plot. However, the secondary weight flow giving optimum net-thrust would, of course, depend upon the source and state of the secondary-air stream for any particular installation.

In general, the shape of either type of thrust curve (for a constant corrected weight-flow ratio) is similar and is a result of the following: As the primary-nozzle pressure ratio is increased from a value of about 2, the thrust coefficient (or the thrust ratio) first decreases because of overexpansion of the flow and then increases as the pressure ratio is further increased and reaches a peak value near the design pressure ratio. (The design pressure ratio is defined as that pressure ratio which would result from isentropic expansion of the flow from the area of the primary nozzle to the area of the shroud exit.) As the primary-nozzle pressure ratio is increased above the value for peak thrust coefficient, the thrust coefficient (or thrust ratio) decreases because of underexpansion losses. For most values of pressure ratio, the value of the ratio of ejector thrust to ideal primary thrust for a given corrected weight-flow ratio is approximately equal to the thrust ratio (or coefficient) for zero secondary flow plus the corrected weight-flow ratio. This indicates that the increase in ejector thrust ratio with secondary weight flow is largely due to the additional mass flow, and reflects the fact that the energy conversion of the combined primary and secondary streams is about the same as that of the primary stream alone.

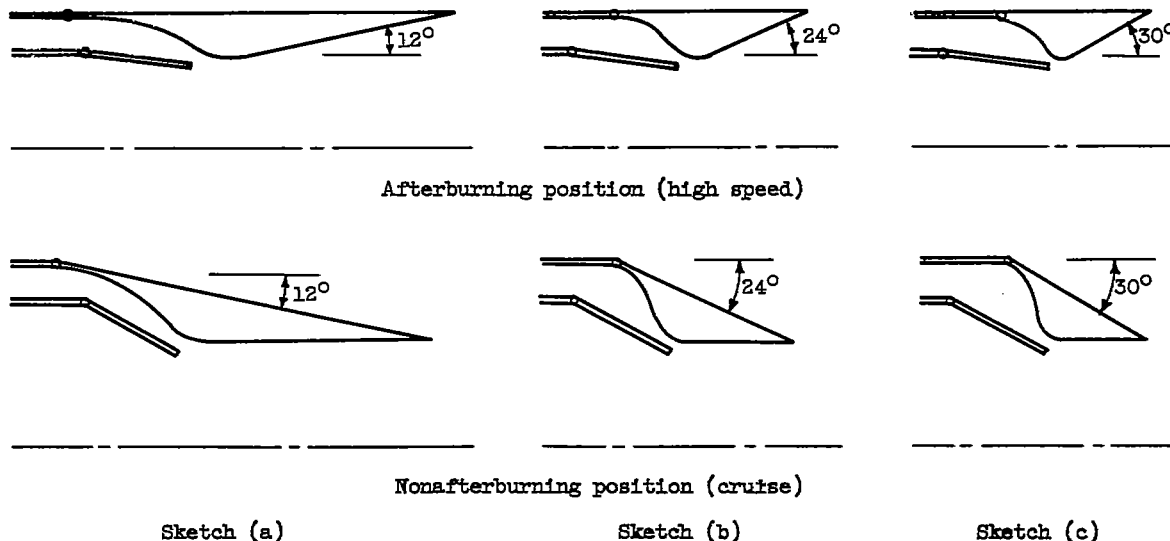
The air-handling characteristics (sometimes referred to as the pumping characteristics) for the ejector models are shown by plots of

ejector total-pressure ratio (ratio of secondary total pressure to primary total pressure) against the primary-nozzle pressure ratio. From these data plots it is possible to determine the amount of secondary airflow the ejector will pass for a given primary-nozzle pressure ratio and secondary-passage total pressure.

The primary-nozzle flow coefficient can be materially affected by secondary flow in some types of ejectors. For divergent-shroud ejectors, however, this effect is small, providing the minimum area of the shroud is not downstream of the primary-nozzle exit. The reduction in primary flow coefficient at the highest secondary weight flow was not greater than 1 percent for all configurations investigated. Primary-nozzle flow coefficients were not affected by changes in divergence angle.

Effect of flow divergence angle on design-point thrust. - In figure 14 the design-point thrust coefficient for zero secondary airflow and for representative weight-flow ratios is plotted against the flow divergence angle (divergence angle from primary exit to shroud exit) for each of the nine configurations tested and also for the three configurations from reference 1. (For each configuration the thrust coefficient for all other corrected weight-flow ratios investigated fell within the limits of the two values shown.) Also shown in figure 14 is a theoretical curve in which the factor $\frac{1}{2} (1 + \cos \alpha)$ is used to approximate the expected decrease in thrust due to the nonaxial component of velocity at the nozzle exit (ref. 2). The flow divergence angle α resulted in a better correlation of data with the theoretical curve than did the shroud divergence angle β .

In a typical variable-geometry ejector-nozzle application, a high shroud divergence angle would represent the maximum flight-speed condition, usually with afterburning (sketch (a)). It may be seen from



Nonafterburning position (cruise)

Sketch (a)

Sketch (b)

Sketch (c)

~~CONFIDENTIAL~~

figure 14 that by increasing the flow divergence angle α from 12° to 24° (sketch (b)) there would be a loss in ejector jet thrust of about 3 percent for any design expansion ratio in the range investigated (exit diameter ratios, 1.24 to 1.82). The decrease in thrust coefficient amounts to another 3 percent as α is increased from 24° to 30° (sketch c). It must be remembered, of course, that, at the very high flight speeds of modern aircraft, the decrease in net thrust can be two or three times greater than the loss in jet thrust.

On the other hand, by increasing α from 12° to 24° , the shroud length would be reduced about 50 percent; and, for a full-scale ejector-nozzle design, this would mean that the shroud surface area which requires cooling would be reduced about 50 percent, with an attendant decrease in weight. Also, for a typical subsonic cruise condition, the shroud of the variable ejector would be closed down in area and become nearly cylindrical in internal shape (see sketches), and the design thrust coefficient would be about 4 percent higher than for the 24° flow divergence angle. This increase in thrust coefficient, however, could be partly or wholly compensated for by an increase in boattail drag resulting from the higher boattail angles associated with the shortened shroud in the closed position for a pod- or nacelle-mounted installation.

The design of an optimum variable-geometry ejector-nozzle configuration thus becomes a complicated process in which the gains to be made in weight saving and cooling requirements for a short high-flow-divergence-angle shroud must be balanced against loss in net thrust at high flight speeds and increase in boattail drag (or base drag) for the cruise condition. Of course, such an analysis must be based on the type of installation (pod-mounted or buried), the flight plan (mostly cruise or mostly high-speed), the take-off procedure (afterburning or nonafterburning), the variation of primary-nozzle geometry, and numerous other factors beyond the scope of this report. It appears from the data of figure 14, however, that the effect of flow divergence angle on internal design-point thrust for divergent-shroud ejectors (generally similar to those examined) can be predicted with reasonable accuracy from theoretical considerations alone.

Effect of shroud divergence angle on thrust coefficient. - In order to illustrate how the shroud divergence angle influences the thrust characteristics of an ejector nozzle, the thrust-coefficient curves for configurations 7 and 9 (β of 15° and 25° , respectively) are shown in figure 15(a) for a typical corrected weight-flow ratio of about 0.032. Both of these models have an exit diameter ratio of approximately 1.8 and a throat diameter ratio of 1.10. The shape of the thrust curves, which is typical for divergent-ejector nozzles and quite similar to that for convergent-divergent nozzles, can be better understood through a knowledge of what is happening to the flow as it passes through the divergent

shroud. One way of doing this is by examining the static-pressure profile along the shroud.

Figure 16 shows the dimensionless axial shroud static-pressure profile for several points along the curves of figure 15. The ambient static-pressure level is indicated for each condition by a dashed line at the right side of the figure. This static-pressure performance map is quite similar to the familiar convergent-divergent nozzle pressure plots (e.g., refs. 3 and 4). As explained in detail in reference 3, any change in thrust of a convergent-divergent nozzle when the throat is choked is brought about by changes in the static-pressure distribution along the divergent walls. A similar situation exists for the divergent ejectors, such that the changes in the thrust-coefficient curves of figure 15 may readily be explained by examining the static-pressure distributions shown in figure 16.

For example, in figure 15(a) at point A for the thrust-coefficient curve of configuration 7 ($\beta = 15^\circ$), the primary jet issues from the choked primary nozzle near ambient pressure and the performance is essentially that of a convergent nozzle. The pressure distribution along the shroud for this condition (fig. 16(a), $P_p/p_0 = 2.56$) is close to ambient pressure, which is represented by the dashed line for $p_0/p_p = 0.391$. The flow through the secondary-passage exit and along the shroud is all subsonic. This is shown by the fact that changes in ambient pressure affect the secondary total pressure at point A in figure 15(b). In this region of operation, then, the primary flow is, in effect, detached from, or not influenced by, the shroud.

Between points A and B in figure 15(a), as the primary-nozzle pressure ratio is increased, the primary jet expands as it leaves the primary nozzle and aspirates the region between the primary jet and the shroud, causing the wall pressures to be lower than ambient along the shroud (e.g., fig. 16(a), $P_p/p_0 = 4.12$), especially near the primary-nozzle exit ($A/A_p = 1.21$). This pressure, lower than ambient, on the divergent area of the shroud creates a force term in the axial direction which opposes (or reduces) the available jet thrust, thus lowering the thrust coefficient.

At point B the primary jet expands until the secondary flow near the shroud becomes choked, and the whole cross-sectional area of the divergent shroud is filled with supersonic flow at some plane downstream of the primary-nozzle exit. Changes in ambient pressure are no longer reflected in the secondary passage as the primary-nozzle pressure ratio is increased (fig. 15(b)). Now, the primary flow is effectively attached to the shroud for a short distance downstream of the primary-nozzle exit,

~~CONFIDENTIAL~~

as shown by the static-pressure profile in figure 16(a) for $P_p/p_0 = 4.58$. For this condition the static-pressure ratio for the first two taps becomes fixed at a minimum value and no longer changes as the nozzle pressure ratio is increased, thus indicating full supersonic flow at these stations. At an area ratio of about 1.8, a shock occurs and the wall pressures rise again toward ambient pressure as the flow travels toward the exit. The entire area of the shroud, however, is considerably below ambient pressure, and the thrust coefficient is thus at a minimum value.

As the primary pressure ratio is increased beyond point B (fig. 15(a)), the flow expands supersonically farther along the shroud until at point C (pressure ratio of approx. 14.08) it has expanded along the entire shroud length and no further changes in wall pressure occur as P_p/p_0 is increased (fig. 16(a)). At point C a large part of the shroud wall is above ambient pressure (dashed line at $p_0/p_p = 0.071$ in fig. 16(a)) so that the overexpansion losses are much smaller than at point B, causing a rise in the thrust-coefficient curve in figure 15(a) from point B to point C.

At point D (fig. 15(a)) the static pressure at the end of the shroud is just equal to the ambient pressure, and the ejector is operating at design pressure ratio. All the shroud area is at pressures above ambient, and the thrust coefficient is a maximum. As the pressure ratio is increased beyond point D, the thrust coefficient decreases because of underexpansion losses. (The static pressure at the exit of the shroud is greater than ambient; and, if the shroud were extended, an additional force in the thrust direction could be realized which is otherwise lost.)

The characteristic shape of the thrust-coefficient curve for configuration 9 ($\beta = 25^\circ$) in figure 15(a) is, in general, the same as that for the lower-angle configuration just discussed. There are several differences (most noticeably the thrust level), however, which are due to the increased shroud angle (from 15° to 25°). In the region from A' to B', the thrust losses due to aspiration (shroud wall pressure reduced below ambient near the primary exit) are less for the high-shroud-angle configuration (at comparable pressure ratios) because of the greater distance separating the shroud and the primary jet at a given distance downstream of the primary-nozzle exit. This may be seen by comparing the pressure distribution for $P_p/p_0 = 4.12$ in figure 16(a) with that for $P_p/p_0 = 4.06$ in figure 16(b). The static pressures on the shroud are much closer to ambient for the high-shroud-angle configuration. The higher-angle shroud also requires a higher primary-nozzle pressure ratio before the jet becomes effectively attached to the shroud. Thus, the pressure ratio at which the cross-sectional area of the shroud just downstream of the primary-nozzle exit first becomes filled with supersonic

~~CONFIDENTIAL~~

flow is increased from about 4.5 (point B, fig. 15(a)) for configuration 7 ($\beta = 15^\circ$) to about 9 (point B', fig. 15(a)) for configuration 9 ($\beta = 25^\circ$). It is interesting to note that in part of the off-design region the high-angle shroud can give much better performance than the lower-angle models. For example, at a pressure ratio of about 4.5 (fig. 15(a)) the thrust coefficient for the 25° shroud is 7 percentage points higher than that for the 15° shroud.

The maximum thrust coefficient for configuration 9 (point D', fig. 15(a)) is lower than that for configuration 7 (point D, fig. 15(a)) because the nonaxial component of velocity at the shroud exit increases as the shroud angle is increased (ref. 2). Comparison of the shroud wall pressures in figures 16(a) and (b) for the completely expanded supersonic-flow case (the bottom curve in each figure) shows this thrust loss as a lowering of the pressures along most of the shroud - especially near the primary-nozzle exit - due to the higher supersonic-flow turning angle required to attach the jet to the shroud near the primary-nozzle exit. If the shroud angle is further increased, point B' in figure 15(a) will move to higher pressure ratios, and the rise in the thrust-coefficient curve from B' to D' will become less pronounced until eventually the performance degenerates to simple convergent-nozzle performance.

Effect of flow divergence angle on air-handling characteristics. - Because one of the functions of the ejector nozzle is to pump secondary cooling air for an engine installation, the so-called pumping characteristics are of interest, especially at conditions of take-off or low-speed cruise (when the source pressure, such as ram air, is insufficient to do the job). In figure 17 the corrected weight-flow ratio is plotted against the flow divergence angle for various constant values of ejector total-pressure ratio $(P_s/P_p)_{ej}$ at primary-nozzle pressure ratios P_p/p_0 of 2, 3, 4, and 6 and above. The data for figure 17 were obtained from configurations 7, 8, 9, and configuration 10 of reference 1, all with D_e/D_p of about 1.82; however, the same characteristics would, in general, apply to any series of conical divergent ejectors with D_s/D_p of approximately 1.10 and similar shroud angles, regardless of shroud length.

For certain conditions of primary-nozzle pressure ratios below 6 and ejector total-pressure ratios less than 0.50 or 0.60, the shroud angle does have an effect on the pumping characteristics (fig. 17). For example, at P_p/p_0 of 2 and P_s/P_p of 0.48 (which might be typical of take-off conditions)(fig. 17(a)), the lowest-angle configuration ($\alpha = 12^\circ$) passes $4\frac{1}{2}$ percent corrected weight flow, the next-higher-angle model ($\alpha = 17^\circ$) passes 2 percent, and the two highest-angle models ($\alpha = 23^\circ$ and 28°) have zero secondary flow at these conditions.

It should be noted, however, that these low primary-nozzle pressure ratios are in the off-design region of operation for most divergent ejectors, and also that the external flow at flight speeds less than design speed can influence the ambient pressure felt by the ejector (ref. 9). For the latter case, the static pressure at the external lip of the shroud should be substituted for p_0 in P_p/p_0 when the ejector performance is estimated. At the higher pressure ratios (fig. 17(d)) which would be representative of operation near the design point, changes in divergence angle do not affect the pumping characteristics.

Effect of secondary airflow on ejector thrust coefficient. - The thrust coefficient of divergent ejectors is influenced by the secondary flow primarily in the region of overexpansion of the primary flow. In order to illustrate the typical effect of secondary flow on ejector performance, the ejector thrust coefficient and the ejector total-pressure ratio for configuration 7 are shown in figure 18 for the highest and the two lowest corrected weight-flow ratios investigated (including zero secondary flow). Because the static pressures along the shroud are again useful in understanding the shape of the thrust curves, the static-pressure distribution plots for the three corrected weight-flow ratios of figure 18 are shown in figure 19. The effect of secondary flow on thrust coefficient can be conveniently examined in three regions of ejector performance: (1) very low primary-nozzle pressure ratios, where the flow near the wall of the divergent shroud is all subsonic; (2) overexpansion, where supersonic flow first fills the cross-sectional area in the shroud just downstream of the primary-nozzle exit; and (3) pressure ratios near the design point.

For very low primary-nozzle pressure ratios (points A, A', and A'', fig. 18(a)), the primary flow is effectively detached from the shroud, as shown by the fact that the shroud wall pressure ratios of figure 19, at primary-nozzle pressure ratios corresponding to points A, A', and A'' (P_p/p_0 of 2.68, 2.56, and 2.04, respectively) have not reached their minimum value (lowest curve) at any point. For zero and low secondary flows (figs. 19(a) and (b), respectively), the shroud pressures are nearly ambient all along the length of the shroud, and the thrust levels (points A and A', fig. 18(a)) are comparatively high. For the high corrected weight-flow ratio of figure 18(a) ($(w_s/w_p)\sqrt{T_s/T_p} = 0.163$), the value of $(P_s/P_p)_{ej}$ is 0.99 (fig. 18(b)), and the ejector is essentially a convergent-divergent nozzle with a throat diameter equal to D_s . For this case, the shroud pressures near the primary-nozzle exit for point A'' in figure 18(a) are very low (as shown in fig. 19(c) for $P_p/p_0 = 2.04$). This indicates relatively high velocities due to overexpansion of the flow in this region and is responsible for the relatively poor thrust coefficient at point A'' in figure 18(a).

As the primary-nozzle pressure ratio is increased from point A to point B (zero secondary airflow, fig. 18(a)), the thrust coefficient falls off rapidly because of the influence of the increasingly expanding primary jet on the shroud pressures (fig. 19(a), $P_p/p_0 = 3.50$) until, at point C, the supersonic primary jet suddenly attaches to the portion of the shroud near the primary-nozzle exit, causing severe reductions in wall pressure due to overexpansion of the flow (e.g., fig. 19(a), $P_p/p_0 = 4.09$). In this region of pressure ratios, the ejector performance with zero secondary airflow becomes discontinuous, as indicated in figure 18 by the vertical dashed lines (i.e., no stable operation is possible between points B and C in fig. 18).

If a small amount of low-energy secondary air is introduced while the ejector is operating in the region of overexpansion, it will act as a cushion, decreasing the sudden expansion losses as the jet leaves the primary nozzle and thereby reducing the thrust loss due to the lowering of shroud wall pressures in the region just downstream of the primary-nozzle exit for pressure ratios between points A' and C' in figure 18. The pressure ratio at which supersonic flow first attaches to the shroud is then increased beyond point C ($P_p/p_0 = 3.5$ for zero flow) to point C' ($P_p/p_0 = 4.58$ for corrected weight-flow ratio of 0.033 in figs. 18 and 19(b)). Also with low secondary airflow, a shock forms in the shroud at a point nearer the primary-nozzle exit for a given value of primary-nozzle pressure ratio, thus decreasing the overexpansion losses at point C' and causing the thrust coefficient in figure 18(a) to be much higher for the low-secondary-airflow curve than for zero flow in this region of primary pressure ratios.

For the high corrected weight-flow ratio ($(w_s/w_p)\sqrt{T_s/T_p} = 0.163$, fig. 18(a)) the secondary flow expands along with the primary jet and helps fill the shroud, thus decreasing the amount of overexpansion experienced by the primary jet with no secondary flow and raising the thrust coefficient over the no-flow case in the region of overexpansion pressure ratios from point C to point D". However, because of the high-energy level of the secondary air for this condition ($P_s = P_p$), the combined primary and secondary stream tends to remain overexpanded at a much lower pressure ratio (point C") than with lower secondary flows.

The peak thrust coefficients with secondary flow (points D' and D", fig. 18(a)) occur at progressively lower primary-nozzle pressure ratios than for zero secondary airflow (point D), because the increased mass flow (primary and secondary) passing through the fixed shroud area reaches ambient static pressure at the end of the shroud at a lower primary-nozzle pressure ratio than when the primary jet is free to expand in the entire area by itself (i.e., increasing the secondary airflow

has the same effect as decreasing the exit diameter ratio D_e/D_p and shifts the whole performance curve laterally toward lower primary-nozzle pressure ratios.

The peak thrust coefficient at point D is slightly lower than at point D' because of expansion losses associated with higher flow angularity at the primary-nozzle exit and attendant lower wall pressures when no secondary flow is present. This may be seen by comparing the completely expanded curves in figures 19(a) and (b). In figure 19(a) the shroud pressure ratios just downstream of the primary-nozzle exit are lower than in figure 19(b). A divergent ejector of this type with no secondary flow is thus analogous to the step nozzles (convergent-divergent) discussed in reference 10 and suffers a similar loss in peak thrust coefficient. For most of the models tested the level of the peak thrust coefficient did not change as the corrected weight-flow ratio was varied from the lowest value to the highest. Exceptions were configurations 1, 2, and 3, which had extremely short shrouds, and configuration 7, for which point D'' is slightly lower in level than point D' (fig. 18(a)).

Reduction of overexpansion losses by means of secondary flow. - In order to show more clearly the effect of secondary airflow on ejector performance in the region of overexpansion at off-design pressure ratios, the maximum decrease in thrust coefficient from the design-pressure-ratio value due to overexpansion (primary-nozzle pressure ratios less than design) is shown in figure 20 for the nine configurations investigated for zero (fig. 20(a)) and approximately 3-percent (fig. 20(b)) secondary airflows. By comparing figures 20(a) and (b) it may be seen that for all shroud angles there is a large reduction in the thrust losses due to overexpansion for the 3-percent secondary-flow data. For ejectors with exit diameter ratios under 1.5, the maximum thrust losses due to overexpansion are reduced 75 percent or more with 3-percent secondary air. For the ejectors with exit diameter ratios of 1.82, the reduction is about 50 percent. The higher weight-flow ratios have a similar effect upon the ejector thrust coefficient in the overexpanded region but to a decreasing extent as the secondary flow is increased.

Figure 20 also indicates a similar reduction in overexpansion losses with increasing shroud divergence angle. The overexpansion losses for the 25° shrouds were only one-half to one-third as large as those for the 15° shrouds. This is due to the reduced aspiration effect for high-angle shrouds discussed previously in connection with figure 15. Thus, a high-angle shroud, even though it has a lower design-point thrust coefficient, might give much better off-design performance at low pressure ratios than a low-divergence-angle shroud.

SUMMARY OF RESULTS

The internal performance characteristics of nine divergent-shroud ejector nozzles were investigated over a range of primary-nozzle pressure ratios and corrected weight-flow ratios. The object of this investigation was to determine the effect upon ejector performance of increasing the shroud divergence angle from 10° to 15° , 20° , and 25° on three, typical, previously reported ejector nozzles. Unheated dry air was used for both primary and secondary flows. However, unpublished NACA data indicate that there are no significant differences in ejector nozzle performance when hot exhaust gas instead of unheated air is used for the primary jet of any given configuration.

The decrease in design-point thrust coefficient with increase in flow divergence angle (angle measured from primary exit to shroud exit) followed very closely a simple relation involving the cosine of the angle. This indicates that design-point thrust performance for conical divergent ejectors (in the range of geometries investigated) can be predicted with reasonable accuracy. The decrease in design-point thrust coefficient due to increasing the flow divergence angle from 12° to 24° was approximately 3 percent, and from 24° to 30° was an additional 3 percent.

Air-handling or pumping characteristics for the ejectors were not changed by increasing the shroud divergence angle except at low primary-nozzle pressure ratios (under 6) where under certain overexpanded conditions the low-angle shroud models would pump small amounts of secondary air but the higher-angle configurations would not.

For off-design operation in the region of overexpansion, the thrust losses due to overexpansion of the flow were twice as great or more with no secondary airflow than with 3-percent secondary flow. Also, the overexpansion losses for the 15° divergent shrouds were two to three times as great as those for the 25° shrouds.

Primary-nozzle flow coefficients for the models tested were not affected by change in shroud divergence angle but were decreased slightly as the secondary airflow was increased. This decrease was less than 1 percent even at the highest secondary weight-flow ratios.

Lewis Flight Propulsion Laboratory
National Advisory Committee for Aeronautics
Cleveland, Ohio, June 21, 1957

APPENDIX A

SYMBOLS

A	area, sq in.
D	diameter, in.
F	jet thrust, lb
F_{ej}	measured ejector jet thrust, lb
F_p	measured jet thrust of primary nozzle, lb
\mathcal{F}	resultant axial force measured by thrust cell, lb
g	acceleration due to gravity, 32.196 ft/sec ²
L	axial distance between exits of primary nozzle and ejector shroud, in.
m	mass flow, slugs/sec
P	absolute total pressure, lb/sq in.
p	absolute static pressure, lb/sq in.
P_u	pressure measured at circumference of upstream face of secondary-air orifice, lb/sq in.
R	gas constant, 53.35 ft-lb/(lb)(°R)
S	distance between outside of primary nozzle and inside of ejector shroud at plane of primary-nozzle exit, in.
T	total temperature, °R
V	velocity, ft/sec
w	weight flow, lb/sec
$w_{a,2}$	measured air flow at station 2, lb/sec
α	flow divergence angle (see sketch, table I), deg
β	angle of shroud divergence from axis, deg

- γ ratio of specific heats (1.4 for cold air)
- δ dimensionless ratio of total pressure to NACA standard sea-level pressure of 14.696 lb/sq in.
- θ dimensionless ratio of total temperature to NACA standard sea-level temperature of 518.7° R

Subscripts:

- b outside of bellmouth inlet
- c center of duct
- e ejector shroud exit
- ej ejector
- i ideal (one-dimensional isentropic flow)
- ip one-dimensional isentropic expansion of primary flow
- is one-dimensional isentropic expansion of secondary flow
- or secondary-air measuring orifice
- p primary stream, primary-nozzle exit
- p' station p', primary-nozzle inlet (fig. 3)
- s secondary stream or station s
- s' station s', secondary-air plenum chamber (fig. 3)
- O free stream or ambient
- 1 station 1 (fig. 2)
- 2 station 2 (fig. 2)

APPENDIX B

METHODS OF CALCULATION

Thrust Coefficient

The ejector thrust coefficient is defined as the ratio of measured ejector thrust to the sum of the ideal (one-dimensional isentropic) thrust of the primary and secondary streams; that is,

$$F_{ej}/(F_{ip} + F_{is})$$

where F_{ej} is defined as

$$F_{ej} = (mV)_e + A_e(p_e - p_0)$$

and V_e is the axial velocity. Values of F_{ej} for each data point were obtained by means of the equation

$$F_{ej} = p_2 \left[\frac{(mV)_1 - A_1(p_b - p_1)}{p_2} \right] + A_2(p_b - p_0) - \mathcal{F}$$

and the measured quantities p_2 , $P_{2,c}$, p_b , p_0 , and \mathcal{F} as follows: The quantity $\left[\frac{(mV)_1 - A_1(p_b - p_1)}{p_2} \right]$ was obtained from $(p_2/P_{2,c})$ by means of a correlation. The correlation had been obtained by integrating the mV profile at station 1 and carefully measuring the quantities A_1 , $(p_b - p_1)$, and p_2 for a number of points over a wide range of values of $(p_2/P_{2,c})$. The calibrated effective pipe area under the labyrinth seals A_2 was measured by blocking off the primary and secondary passages and noting the variation of \mathcal{F} with $(p_b - p_0)$. The area A_2 was then calculated as

$$A_2 = \mathcal{F}/(p_b - p_0)$$

The ideal primary thrust F_{ip} is defined as the product of the measured primary weight flow and the isentropic velocity corresponding to the measured primary-nozzle pressure ratio:

$$F_{ip} = (m\sqrt{gRT})_p \left(\frac{V}{\sqrt{gRT}} \right)_{ip}$$

where

$$\left(\frac{V}{\sqrt{gRT}}\right)_{ip} = \sqrt{\frac{2\gamma}{\gamma-1} \left[1 - \left(\frac{P_0}{P_p}\right)^{\frac{\gamma-1}{\gamma}} \right]}$$

and

$$(m\sqrt{gRT})_p = K \frac{P_2 A_2}{\left(\frac{pA}{m\sqrt{gRT}}\right)_{2,c}}$$

The symbols p_2 and A_2 are measured values,

$$\left(\frac{pA}{m\sqrt{gRT}}\right)_{2,c} = \frac{\left(\frac{P_2}{P_{2,c}}\right)^{\frac{\gamma-1}{\gamma}}}{\sqrt{\frac{2\gamma}{\gamma-1} \left[1 - \left(\frac{P_2}{P_{2,c}}\right)^{\frac{\gamma-1}{\gamma}} \right]}}$$

and K is an experimentally determined constant which is equal to the ratio of $\left(\frac{pA}{m\sqrt{gRT}}\right)_{2,c}$ and the integrated value of the parameter $\left(\frac{pA}{m\sqrt{gRT}}\right)$

at station 2. The value of K was found to be constant for a range of Mach numbers.

The ideal secondary thrust is defined as the product of the measured secondary weight flow and the isentropic velocity corresponding to the measured secondary pressure ratio $\frac{P_0}{P_s}$:

$$F_{is} = (m\sqrt{gRT})_s \left(\frac{V}{\sqrt{gRT}}\right)_{is}$$

where

$$\left(\frac{V}{\sqrt{gRT}}\right)_{is} = \sqrt{\frac{2\gamma}{\gamma-1} \left[1 - \left(\frac{P_0}{P_s}\right)^{\frac{\gamma-1}{\gamma}} \right]}$$

~~CONFIDENTIAL~~

and

$$(m\sqrt{gRT})_s = p_u \left(\frac{m\sqrt{gRT}}{p} \right)_{or}$$

The term $\left(\frac{m\sqrt{gRT}}{p} \right)_{or}$ was measured at the secondary-air orifice by means of the equation

$$\left(\frac{m\sqrt{gRT}}{p} \right)_{or} = K'Y \sqrt{\frac{2(\Delta p)_{or}}{p_u}}$$

where Y is the expansion factor for the orifice assembly which was used in the secondary-air line; and K' is a constant which includes orifice area, discharge coefficient, and velocity of approach factor and was assumed constant over the range of Reynolds numbers covered in this investigation. The pressure p_u is the pressure measured at the circumference of the upstream face of the orifice, and $(\Delta p)_{or}$ is the pressure difference between the upstream and downstream faces of the orifice (ref. 11).

Weight-Flow Ratio

The corrected weight-flow ratio was calculated as

$$\frac{w_s}{w_p} \sqrt{\frac{T_s}{T_p}} = \frac{(m\sqrt{gRT})_s}{(m\sqrt{gRT})_p}$$

Primary-Nozzle Discharge Coefficient

The primary-nozzle discharge coefficient was defined as the ratio of actual-to-ideal corrected weight-flow parameters; that is,

$$\left(\frac{w_{a,2} \sqrt{\theta_p}}{A_p \delta_p} \right) / \left(\frac{w \sqrt{\theta}}{A \delta} \right)_i$$

where

$$w_{a,2} = 32.2 (m\sqrt{gRT})_p / (\sqrt{gRT})_p$$

and

~~CONFIDENTIAL~~

$$\left(\frac{w\sqrt{\theta}}{A\delta}\right)_i = 14.696 \sqrt{\frac{2\gamma}{(\gamma-1)R(518.7)}} \left[\left(\frac{P_0}{P_p}\right)^{\frac{2}{\gamma}} - \left(\frac{P_0}{P_p}\right)^{\frac{\gamma+1}{\gamma}} \right]^{1/2}$$

for unchoked values of primary-nozzle pressure ratio. For primary-nozzle pressure ratios above the theoretical choking value, the ideal weight-flow parameter was assumed constant at the critical value of 0.3432 pound per second per square inch for $\gamma = 1.4$.

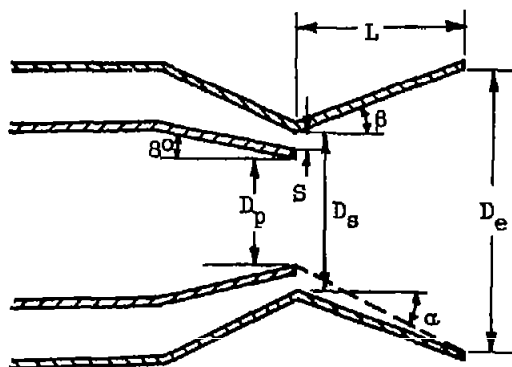
REFERENCES

1. Greathouse, William K., and Beale, William T.: Performance Characteristics of Several Divergent-Shroud Aircraft Ejectors. NACA RM E55G21a, 1955.
2. Steffen, Fred W., Krull, H. George, and Schmiedlin, Ralph F.: Effect of Divergence Angle on the Internal Performance Characteristics of Several Conical Convergent-Divergent Nozzles. NACA RM E54H25, 1954.
3. Krull, H. George, and Steffen, Fred W.: Performance Characteristics of One Convergent and Three Convergent-Divergent Nozzles. NACA RM E52H12, 1952.
4. Schairer, G.: Performance Characteristics of Jet Nozzles. Doc. No. D-12054, Boeing Airplane Co., Seattle (Wash.), July 25, 1951.
5. Huntley, S. C., and Yanowitz, Herbert: Pumping and Thrust Characteristics of Several Divergent Cooling-Air Ejectors and Comparison of Performance with Conical and Cylindrical Ejectors. NACA RM E53J13, 1954.
6. Greathouse, W. K.: Preliminary Investigation of Pumping and Thrust Characteristics of Full-Size Cooling-Air Ejectors at Several Exhaust-Gas Temperatures. NACA RM E54A18, 1954.
7. Campbell, Carl E., and Sobolewski, Adam E.: Altitude-Chamber Investigation of J73-GE-1A Turbojet Engine Component Performance. NACA RM E53I08, 1954.
8. Wallner, Lewis E., and Wintler, John T.: Experimental Investigation of Typical Constant- and Variable-Area Exhaust Nozzles and Effects on Axial-Flow Turbojet-Engine Performance. NACA RM E51D19, 1951.

9. Valerino, Alfred S., and Yeager, Richard A.: External-Stream Effects on Gross Thrust and Pumping Characteristics of Ejectors Operating at Off-Design Mach Numbers. NACA RM E56C14, 1956.
10. Steffen, Fred W., Krull, H. George, and Schmiedlin, Ralph F.: Effects of Several Geometric Variables on Internal Performance of Short Convergent-Divergent Exhaust Nozzles. NACA RM E54L09, 1955.
11. Anon.: Standards for Discharge Measurement with Standardized Nozzles and Orifices. NACA TM 952, 1940.

UN

TABLE I. - EJECTOR CONFIGURATIONS



Configu- ration	Primary-nozzle diameter, D_p , in.		Exit diameter ratio, D_e/D_p	Throat diameter ratio, D_s/D_p	Annulus ratio, S/D_p	Spacing ratio, L/D_p	Shroud divergence angle, β , deg	Flow divergence angle, α , deg	Data in fig- ure -
	Inside	Outside							
1	8.30	8.55	1.24	1.08	0.024	0.38	15	18	5
2	8.30	8.55	1.24	1.08	.024	.28	20	23	6
3	8.30	8.55	1.24	1.08	.024	.22	25	28	7
^a (3)	(6.02)	(6.14)	(1.23)	(1.04)	(.010)	(.47)	(12)	(14)	
4	8.30	8.55	1.46	1.10	.036	.69	15	19	8
5	8.30	8.55	1.46	1.10	.036	.51	20	25	9
6	8.30	8.55	1.46	1.10	.036	.40	25	30	10
^a (5)	(6.02)	(6.14)	(1.45)	(1.09)	(.035)	(1.06)	(9)	(12)	
7	6.50	6.63	1.82	1.10	.038	1.31	15	17	11
8	6.50	6.63	1.81	1.10	.038	.98	20	23	12
9	6.50	6.63	1.81	1.10	.038	.76	25	28	13
^a (10)	(6.02)	(6.14)	(1.82)	(1.10)	(.040)	(1.90)	(11)	(12)	

^aNumbers in parentheses refer to values for three configurations of ref. 1.

TABLE II. - INSTRUMENTATION

Station or location (figs. 2 and 3)	Total pressure	Static pressure
1	6-Probe equal-area rake; 5-probe boundary-layer survey	2 Wall taps
Outside of bellmouth inlet	---	7-Probe longitudinal survey
2	2 Radial 7-probe equal-area rakes, 180° apart; 4-probe boundary-layer survey	4 Wall taps
p' (Primary-nozzle inlet)	14-Probe equal-area diametral rake	---
s	Single probe	---
s' (Secondary-air plenum chamber)	One 3-probe rake and 3 single probes, all spaced 90° apart	---
Ejector shroud (inside surface)	---	Axial survey, taps approx. 1 in. apart
O (Tank, ambient)	---	2 Wall taps

4400

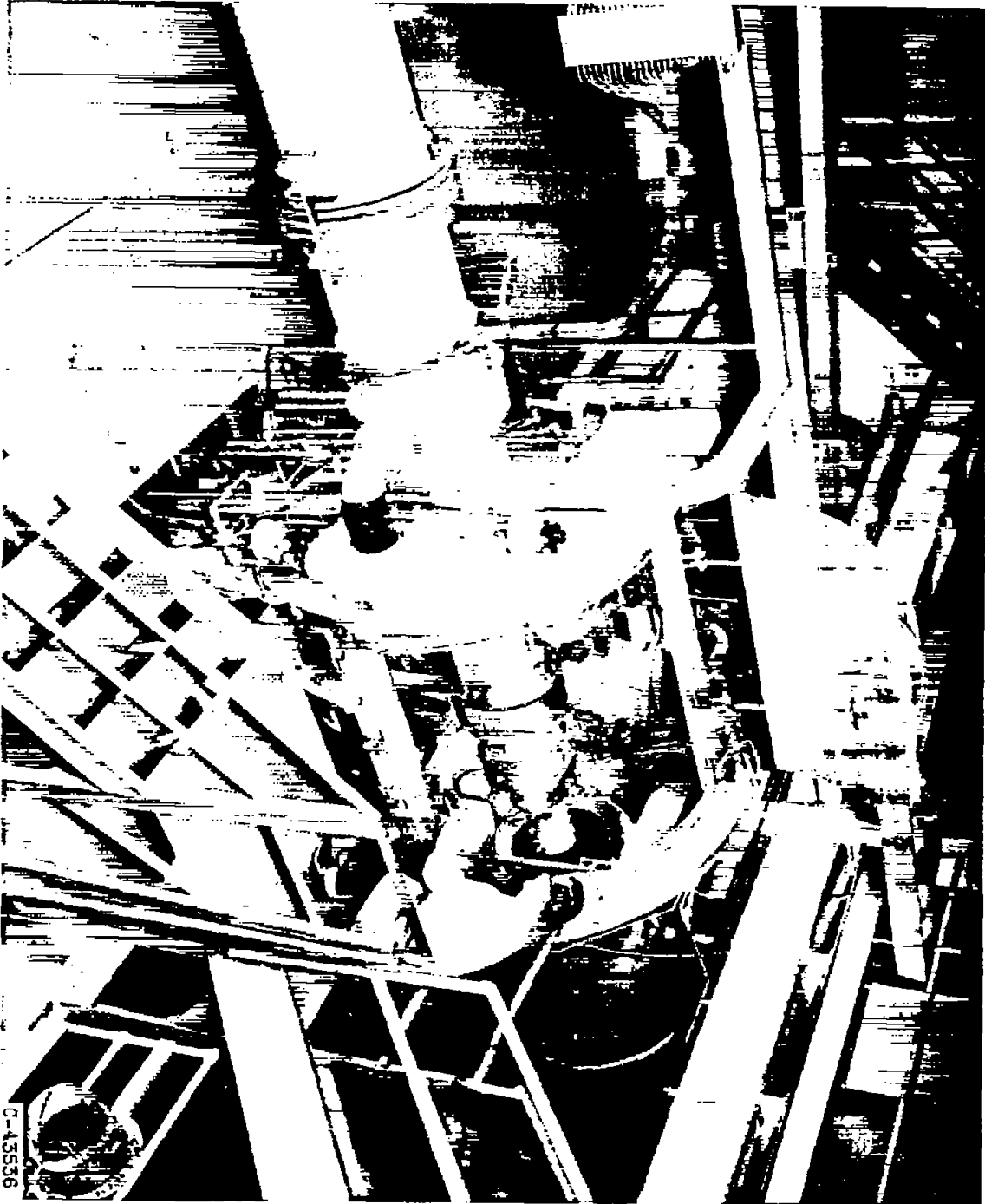


Figure 1. - Test facility.

C-43336

OP-4

4400

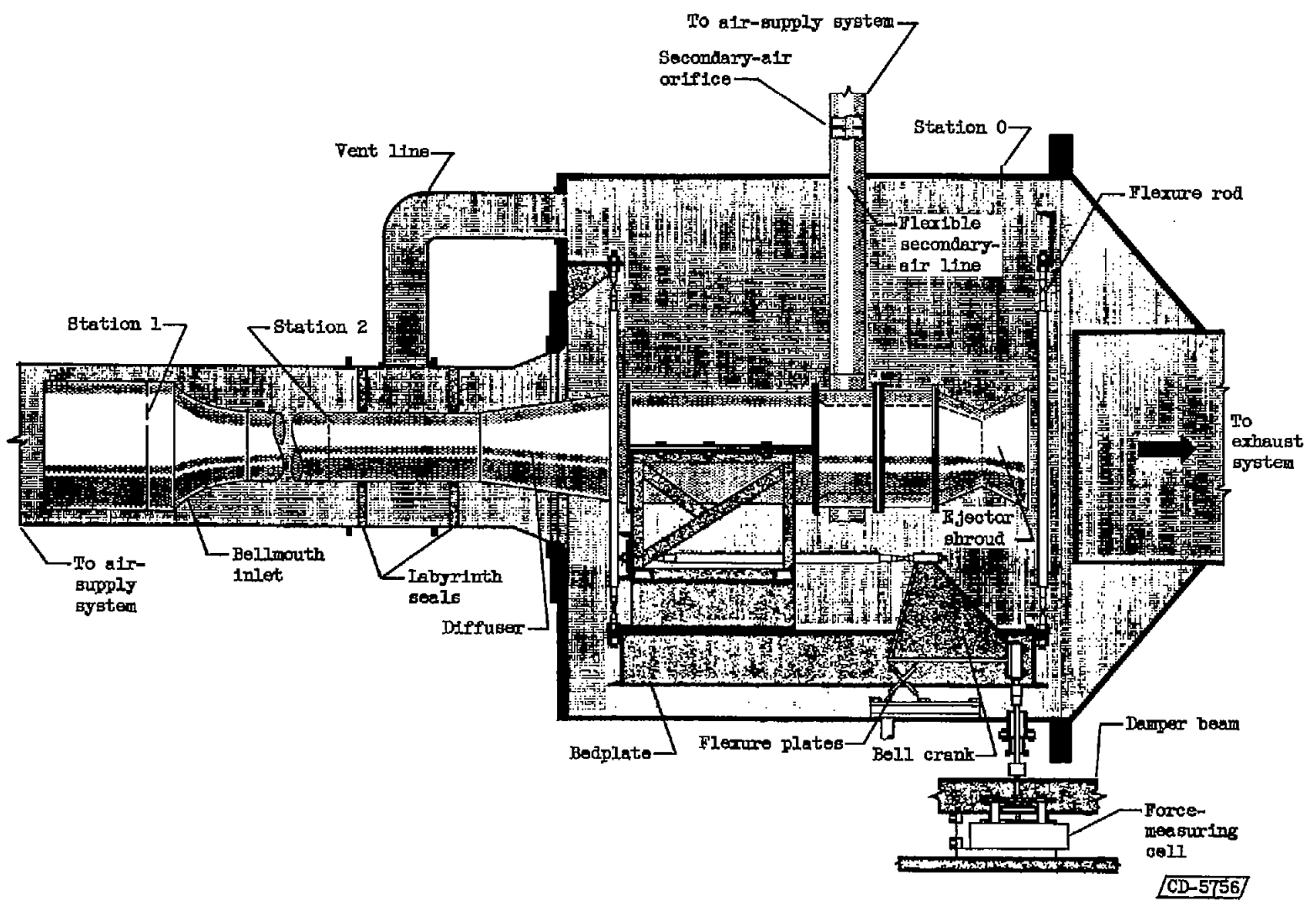


Figure 2. - Schematic diagram of ejector-nozzle test facility.

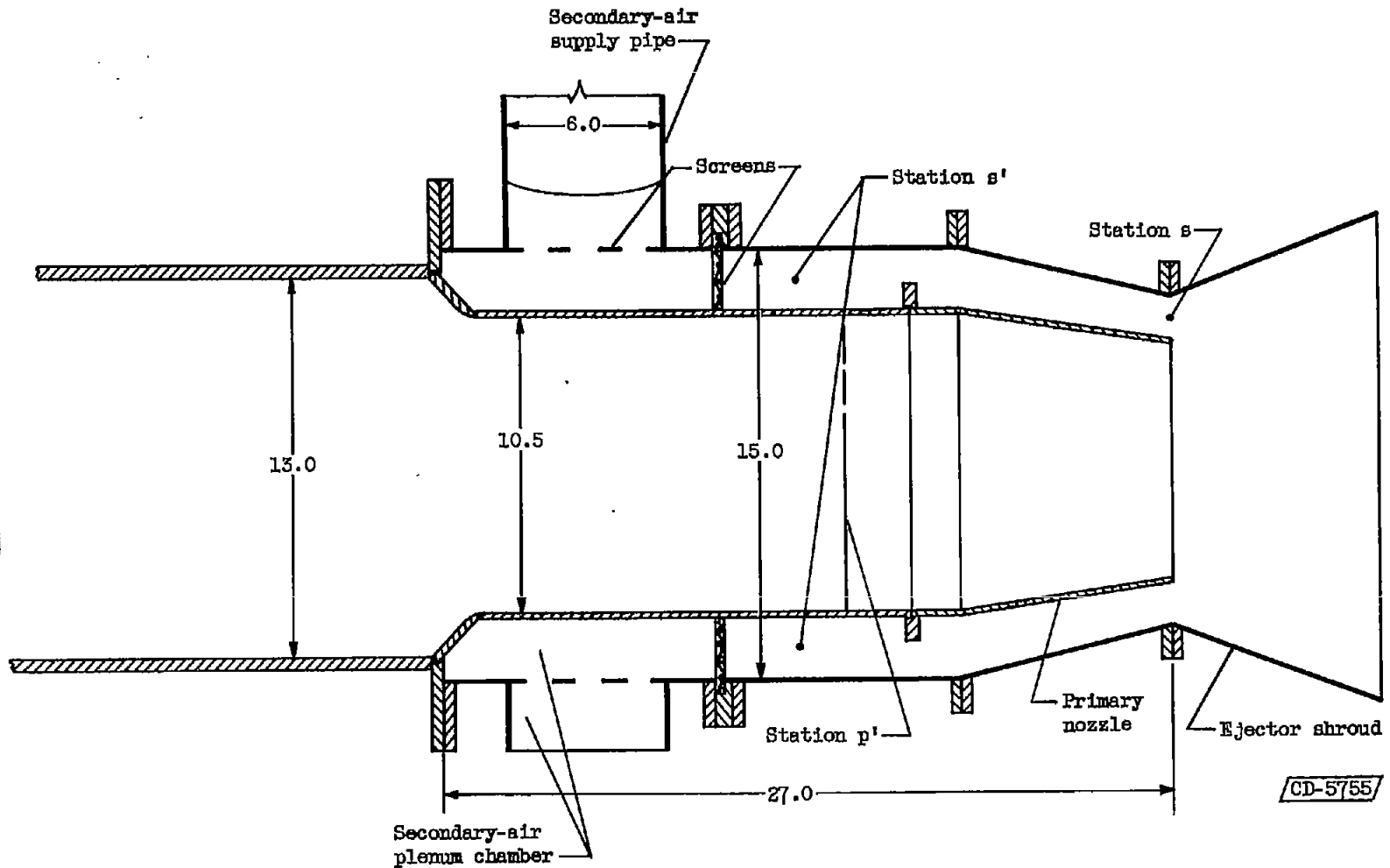


Figure 3. - Schematic diagram of typical ejector assembly. (All dimensions in inches.)

4400

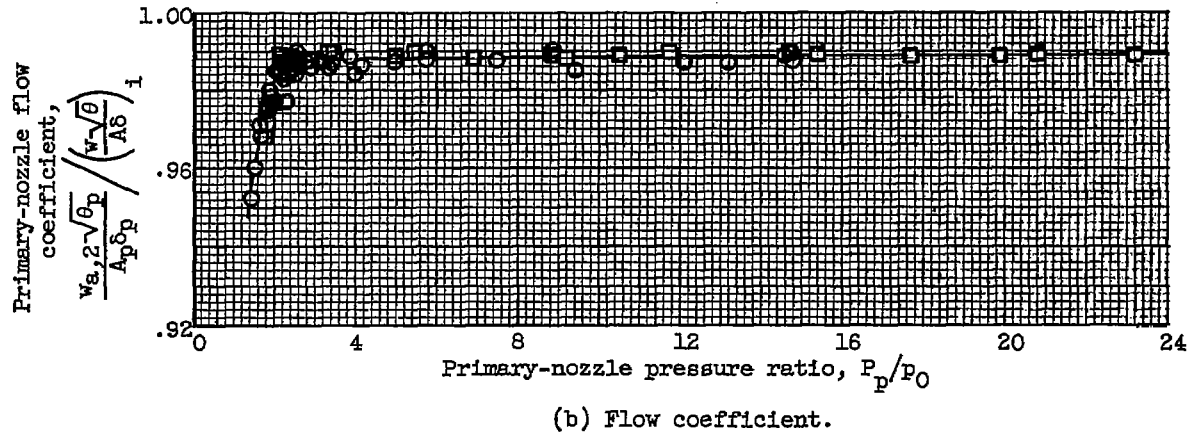
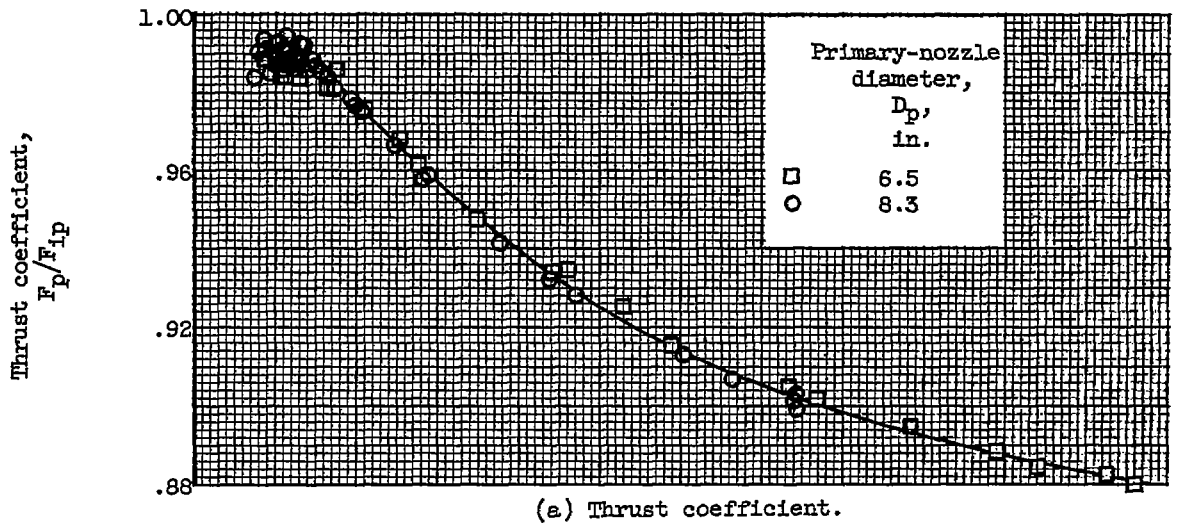
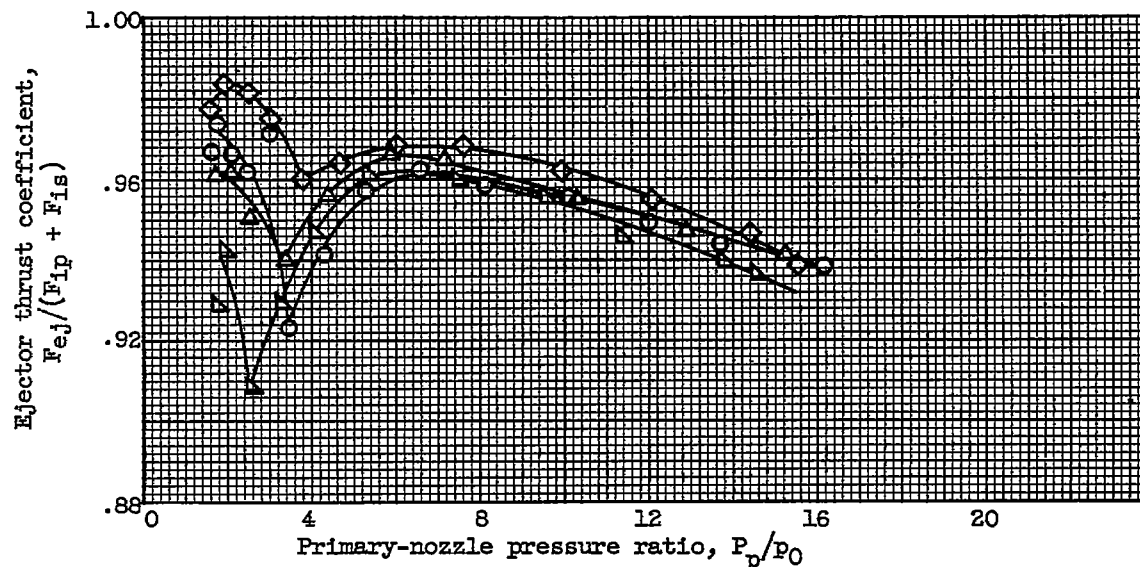
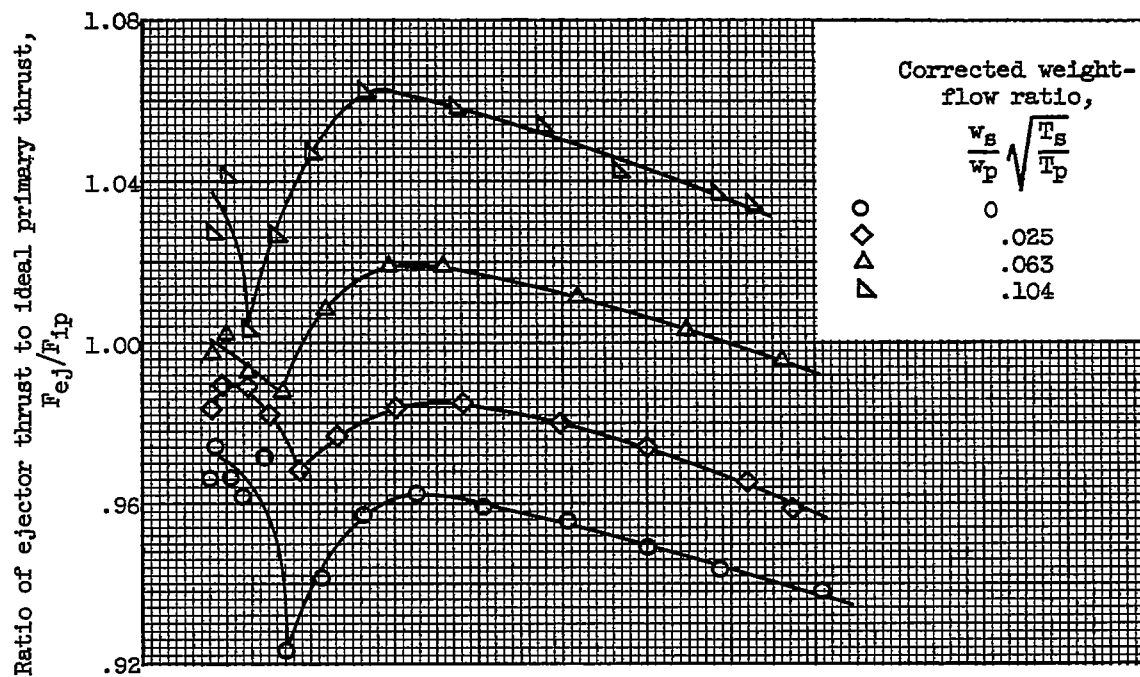


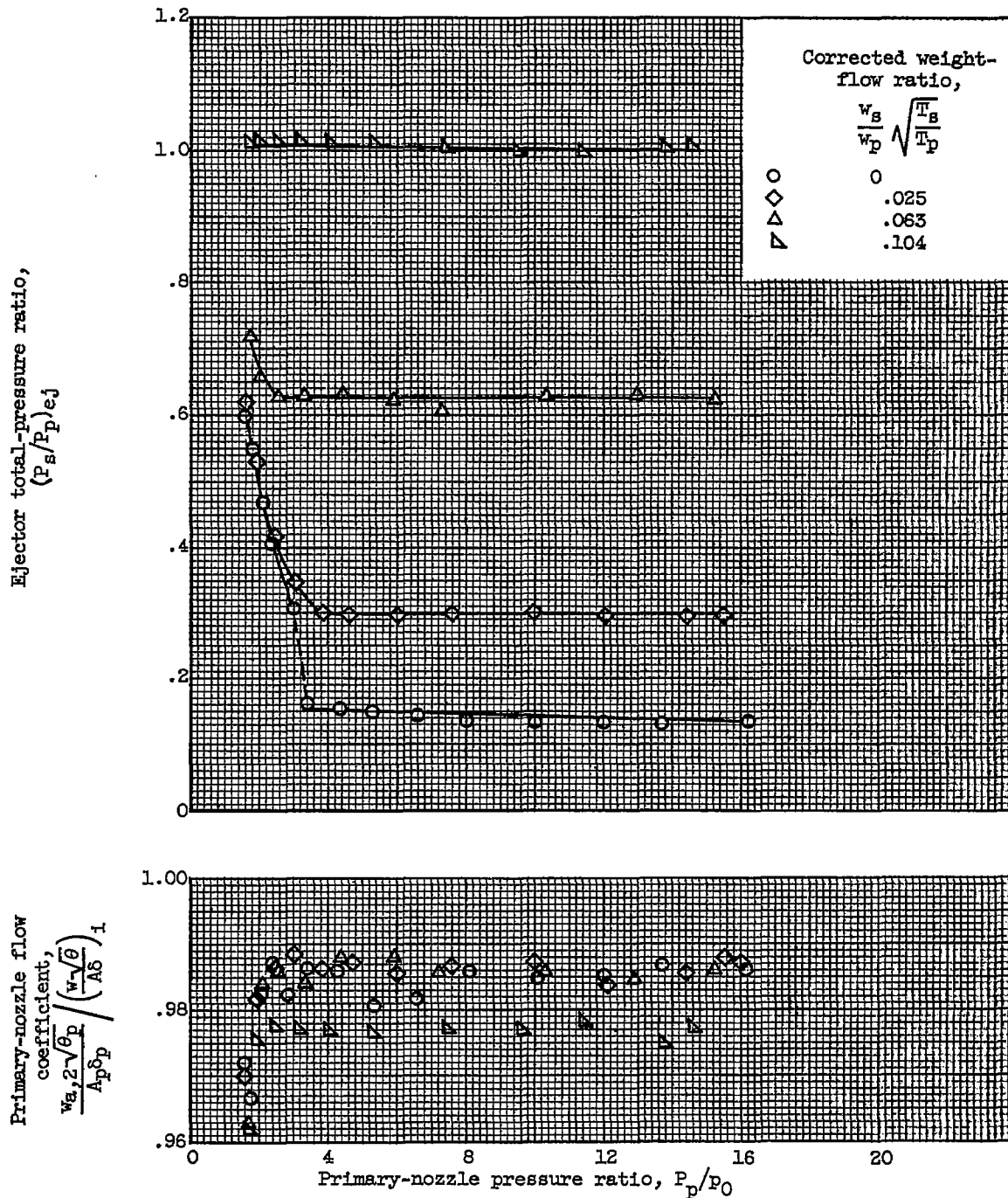
Figure 4. - Performance of primary nozzles (no ejector shroud).

4400



(a) Thrust characteristics.

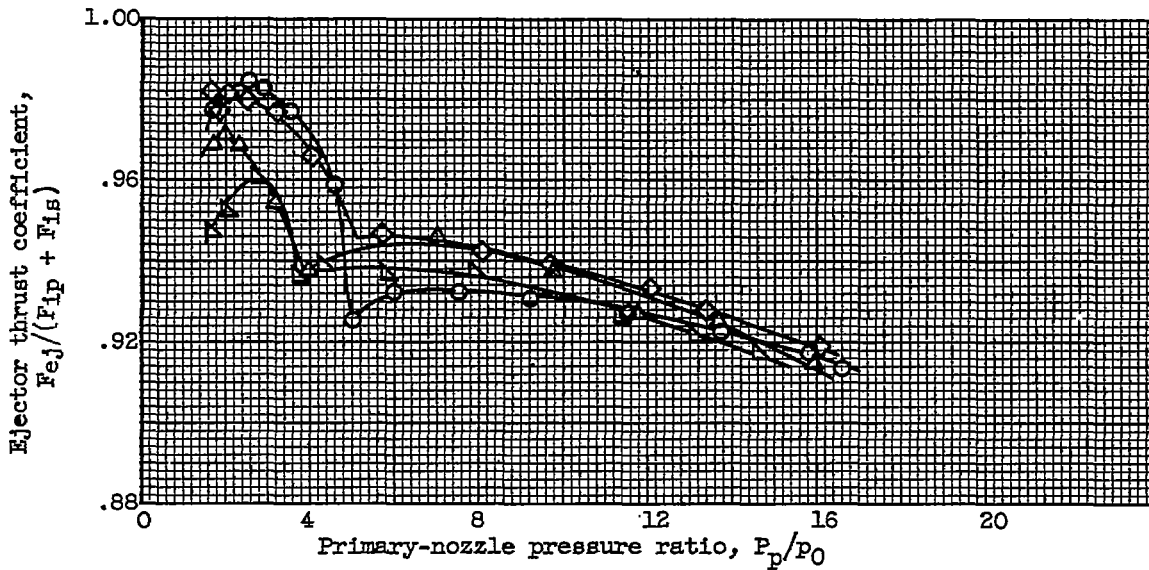
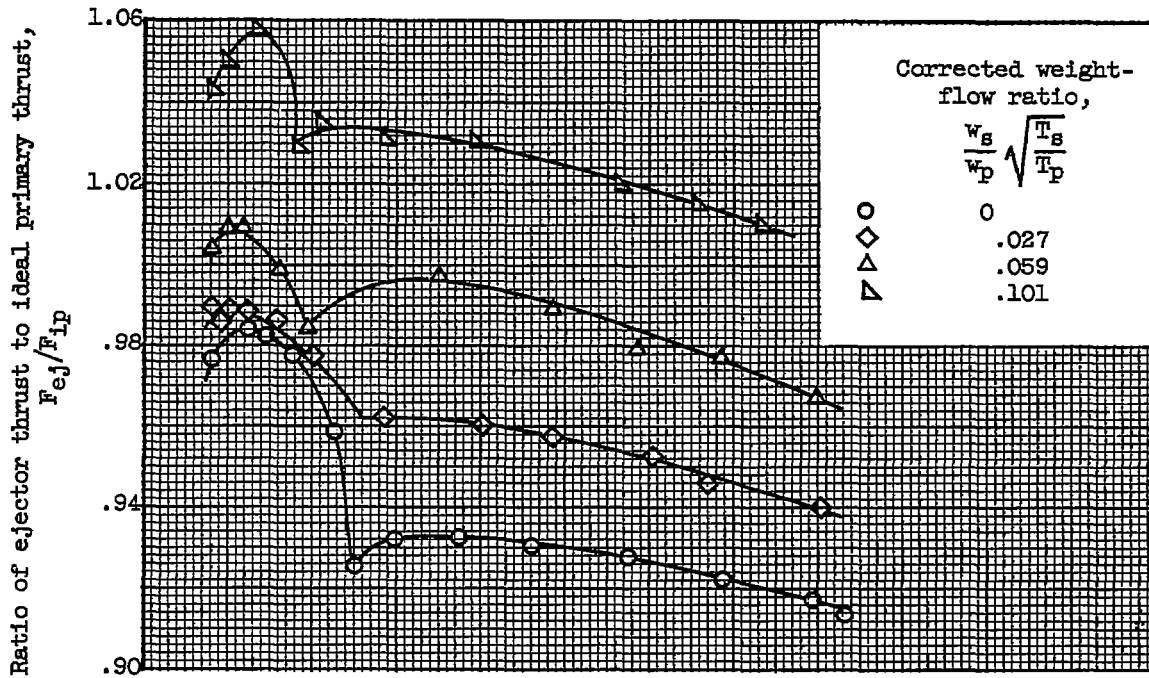
Figure 5. - Performance of ejector 1. Exit diameter ratio, 1.24; throat diameter ratio, 1.08; spacing ratio, 0.38; flow divergence angle, 18°; shroud divergence angle, 15°.



(b) Flow characteristics.

Figure 5. - Concluded. Performance of ejector 1. Exit diameter ratio, 1.24; throat diameter ratio, 1.08; spacing ratio, 0.38; flow divergence angle, 18° ; shroud divergence angle, 15° .

4400



(a) Thrust characteristics.

Figure 6. - Performance of ejector 2. Exit diameter ratio, 1.24; throat diameter ratio, 1.08; spacing ratio, 0.28; flow divergence angle, 23° ; shroud divergence angle, 20° .

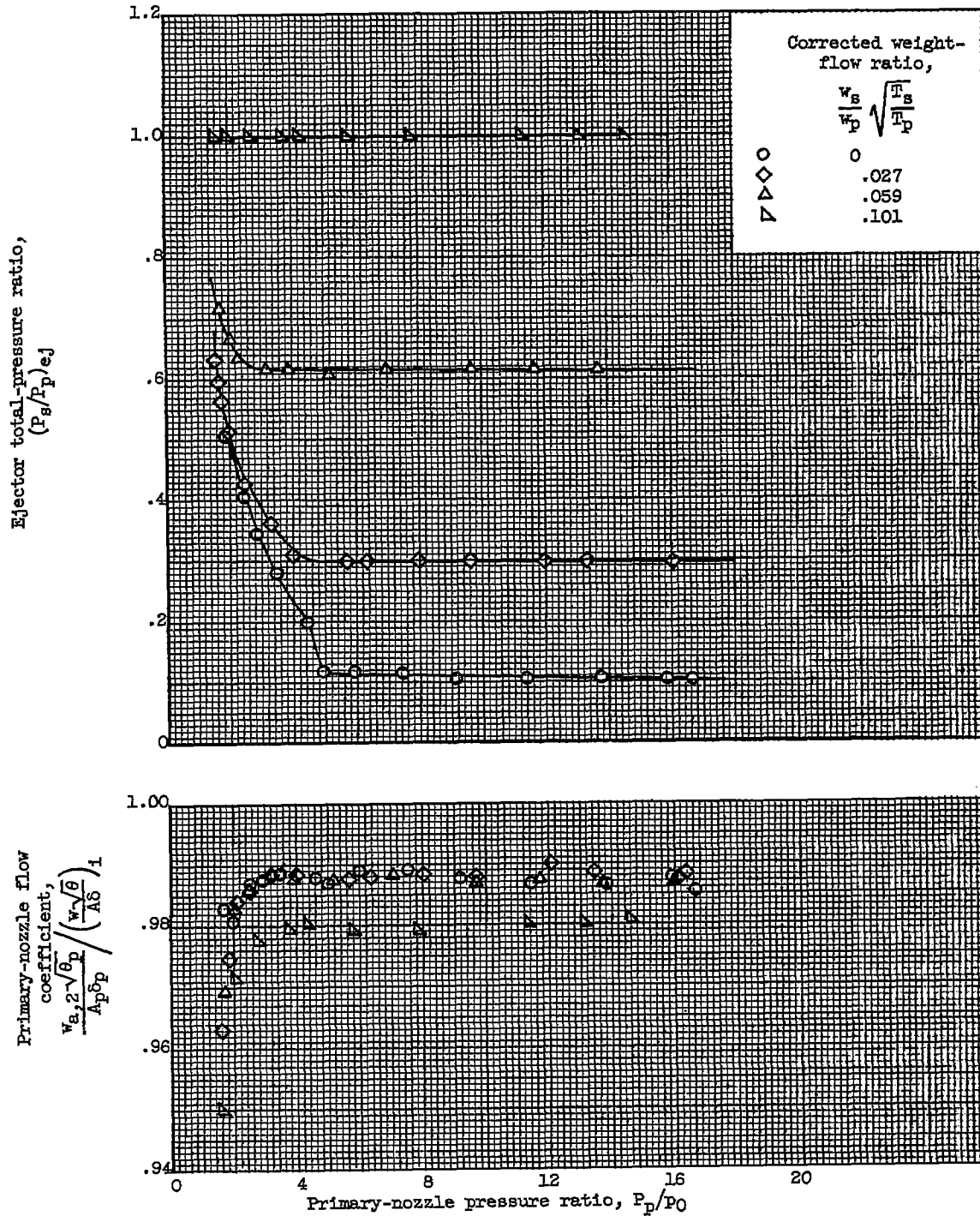
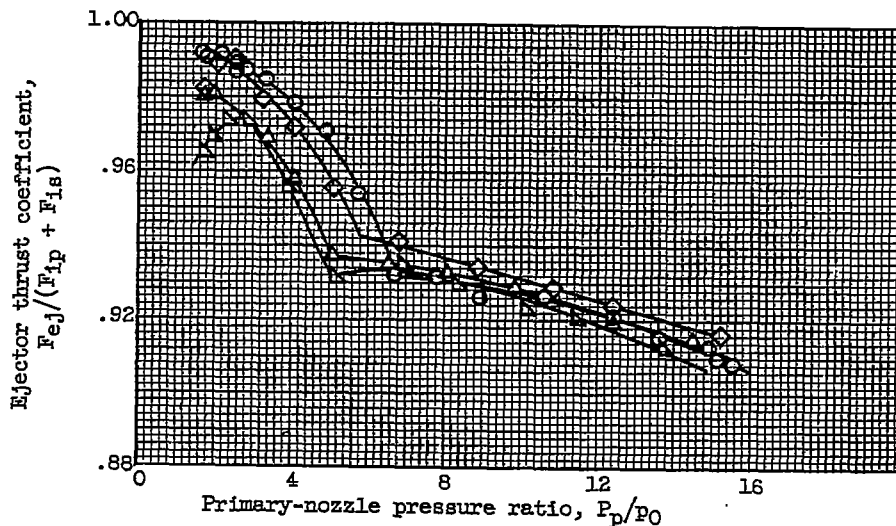
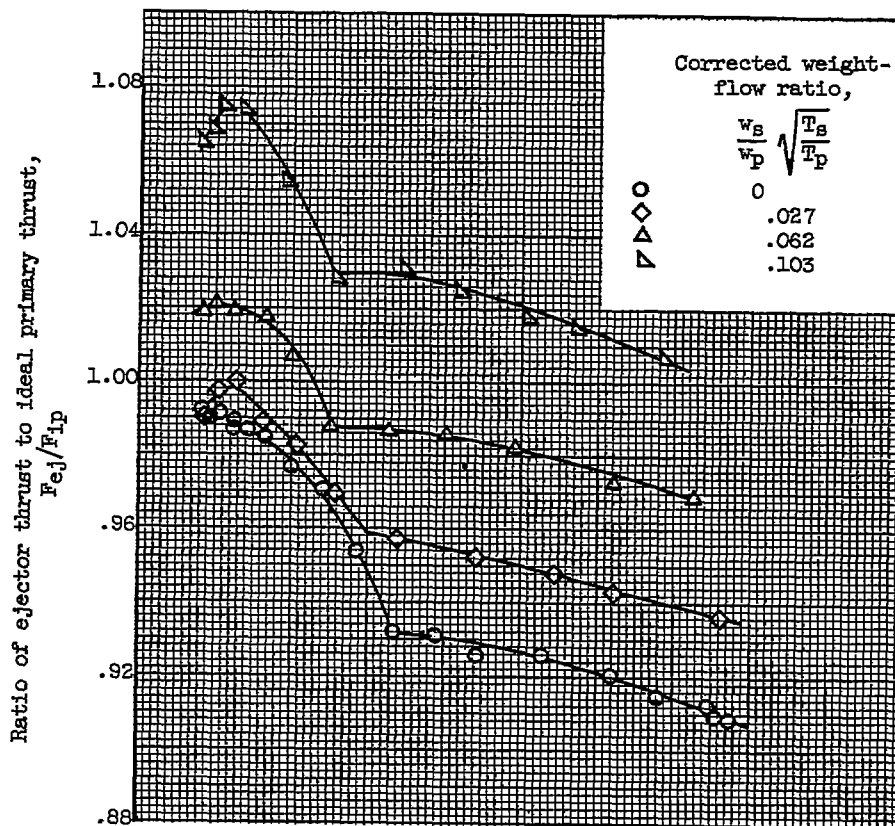
~~CONFIDENTIAL~~

Figure 6. - Concluded. Performance of ejector 2. Exit diameter ratio, 1.24; throat diameter ratio, 1.08; spacing ratio, 0.28; flow divergence angle, 23°; shroud divergence angle, 20°.

~~CONFIDENTIAL~~

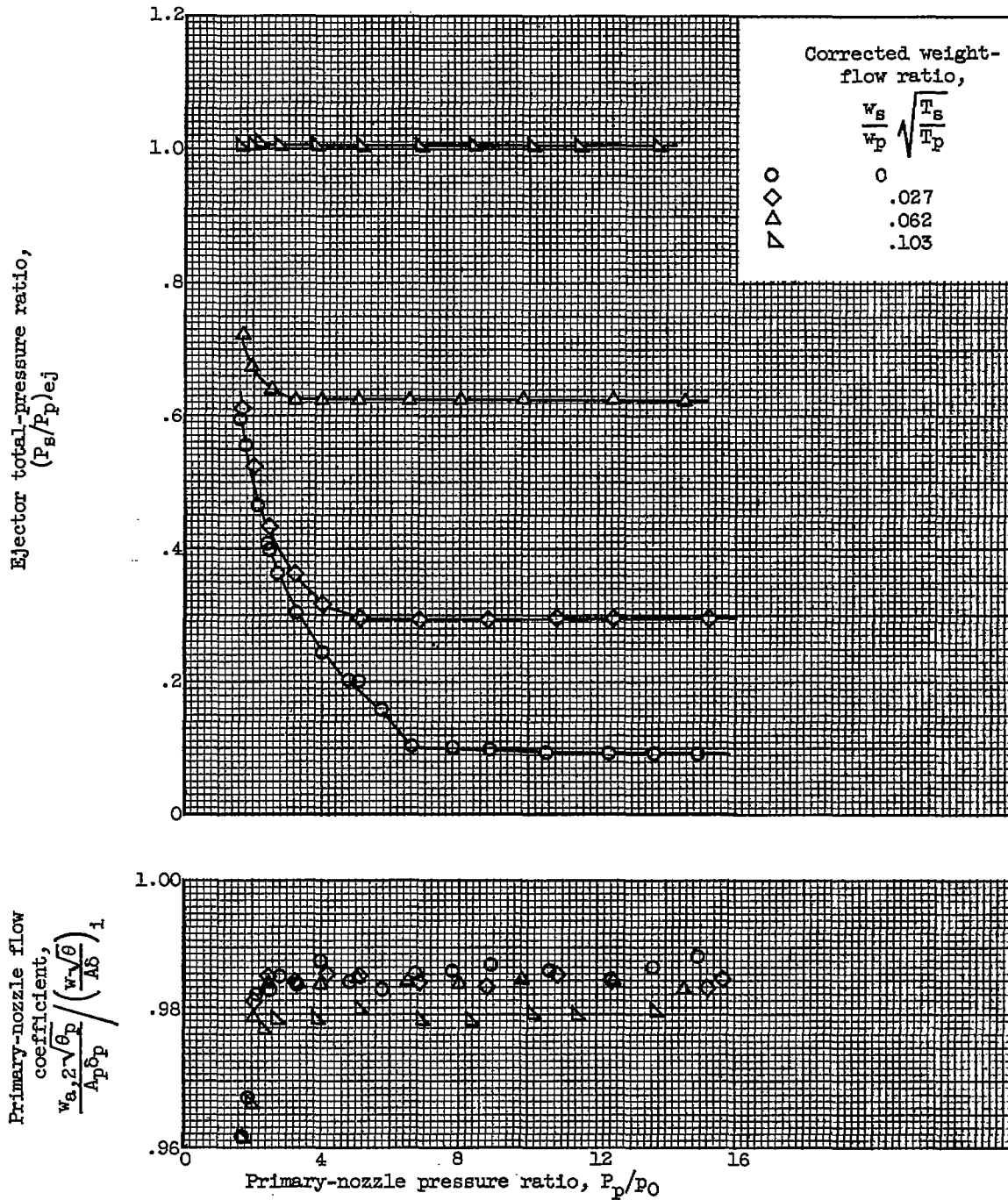
CP-5
4400



(a) Thrust characteristics.

Figure 7. - Performance of ejector 3. Exit diameter ratio, 1.24; throat diameter ratio, 1.08; spacing ratio, 0.22; flow divergence angle, 28°; shroud divergence angle, 25°.

CONFIDENTIAL

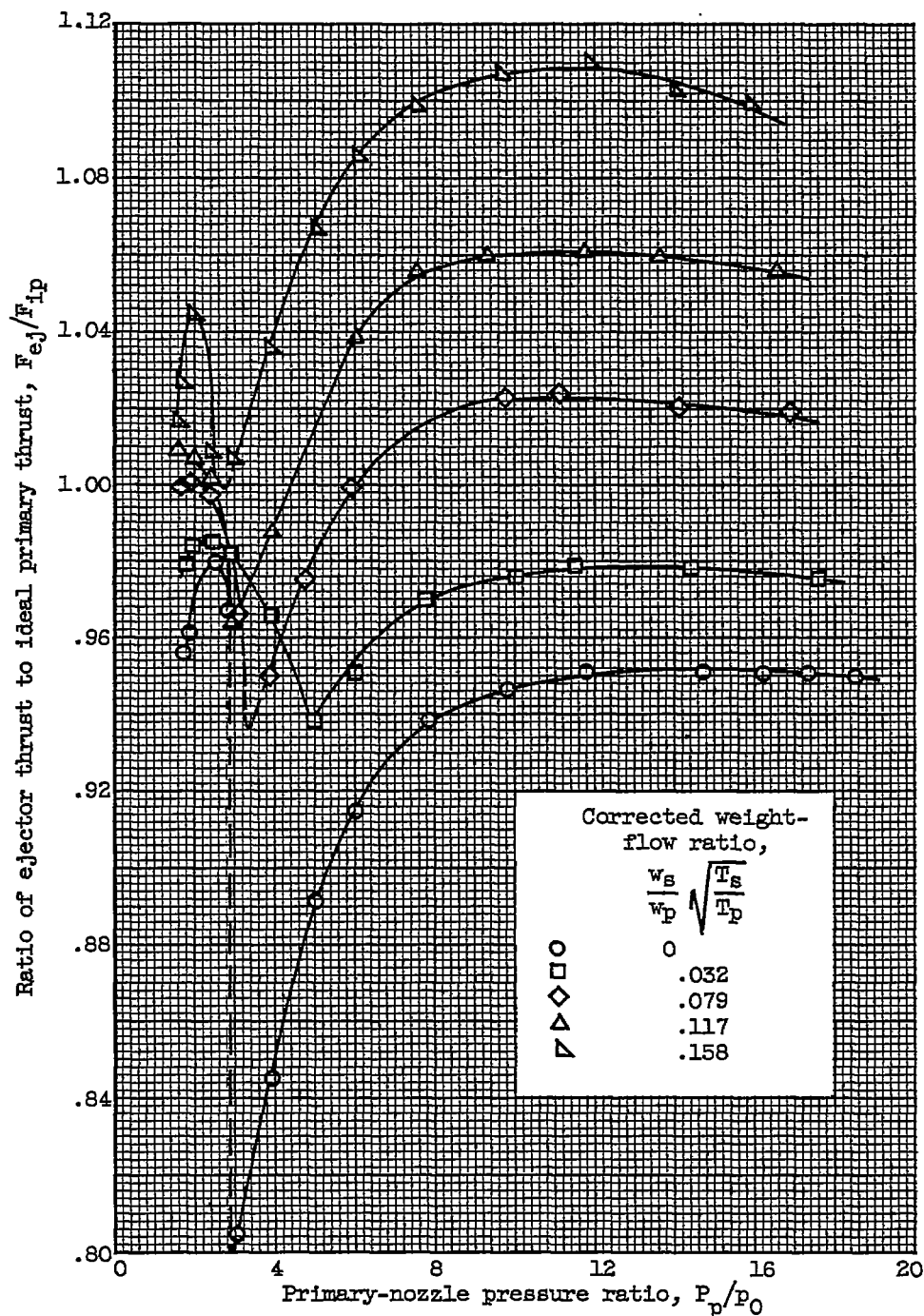
~~CONFIDENTIAL~~

(b) Flow characteristics.

Figure 7. - Concluded. Performance of ejector 3. Exit diameter ratio, 1.24; throat diameter ratio, 1.08; spacing ratio, 0.22; flow divergence angle, 28° ; shroud divergence angle, 25° .

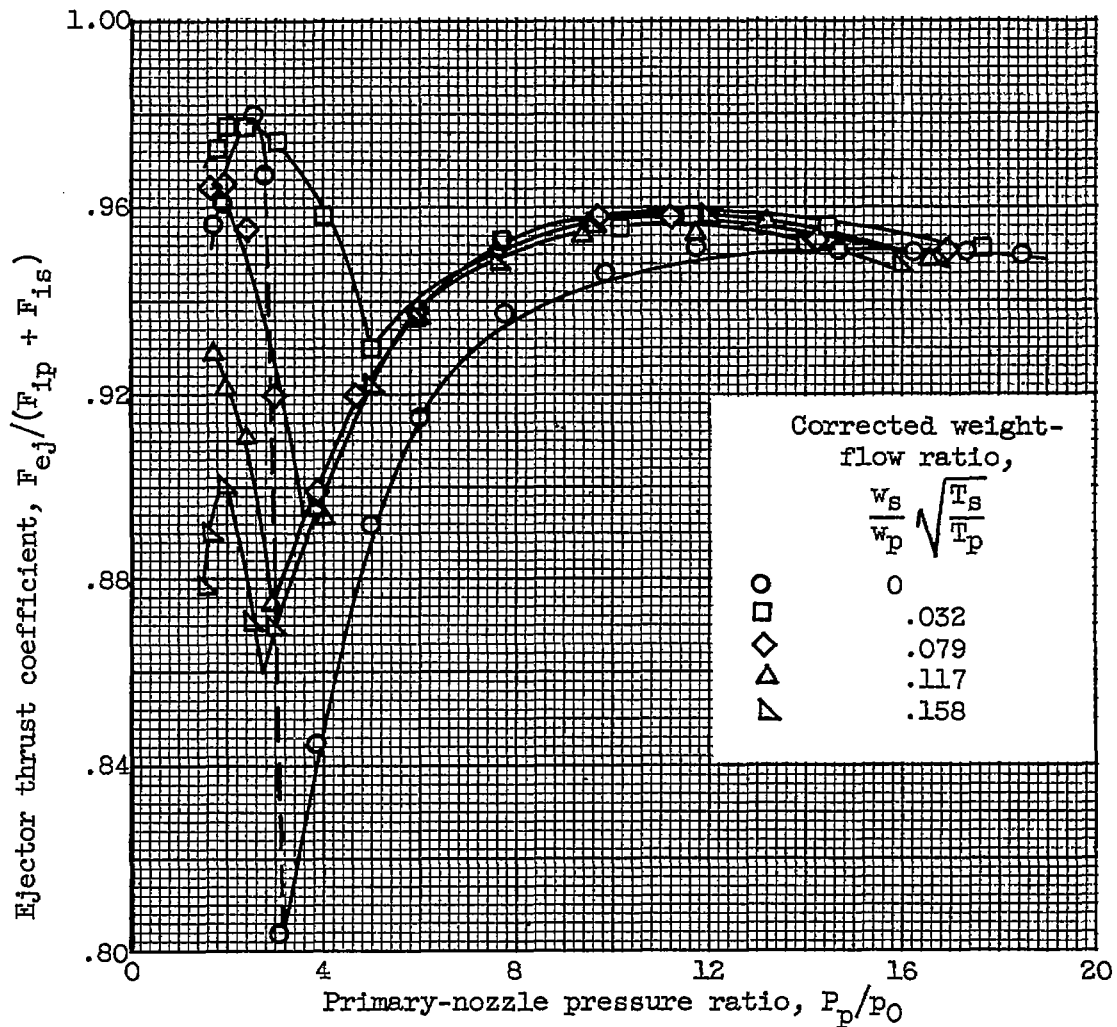
~~CONFIDENTIAL~~

CP-5 back 4400



(a) Thrust characteristics.

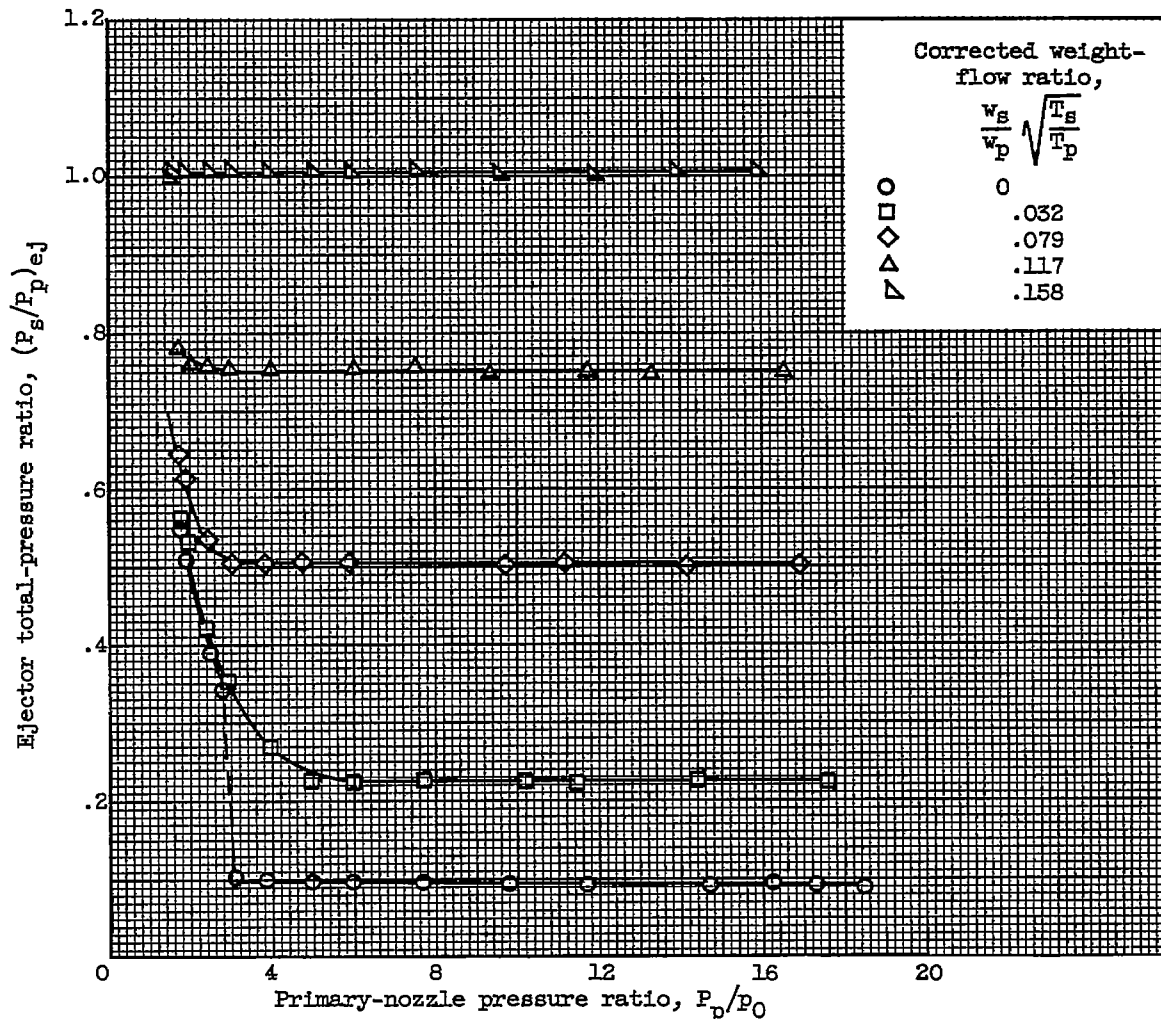
Figure 8. - Performance of ejector 4. Exit diameter ratio, 1.46; throat diameter ratio, 1.10; spacing ratio, 0.69; flow divergence angle, 19°; shroud divergence angle, 15°.



(a) Concluded. Thrust characteristics.

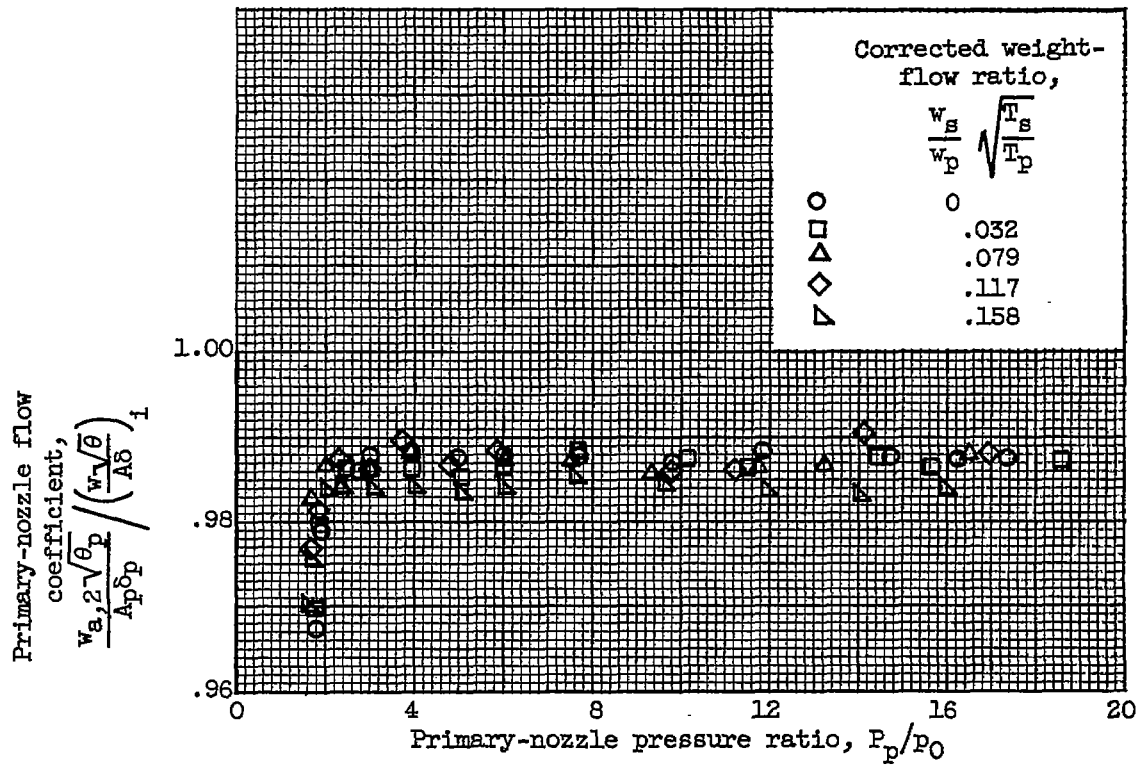
Figure 8. - Continued. Performance of ejector 4. Exit diameter ratio, 1.46; throat diameter ratio, 1.10; spacing ratio, 0.69; flow divergence angle, 19° ; shroud divergence angle, 15° .

4400



(b) Flow characteristics.

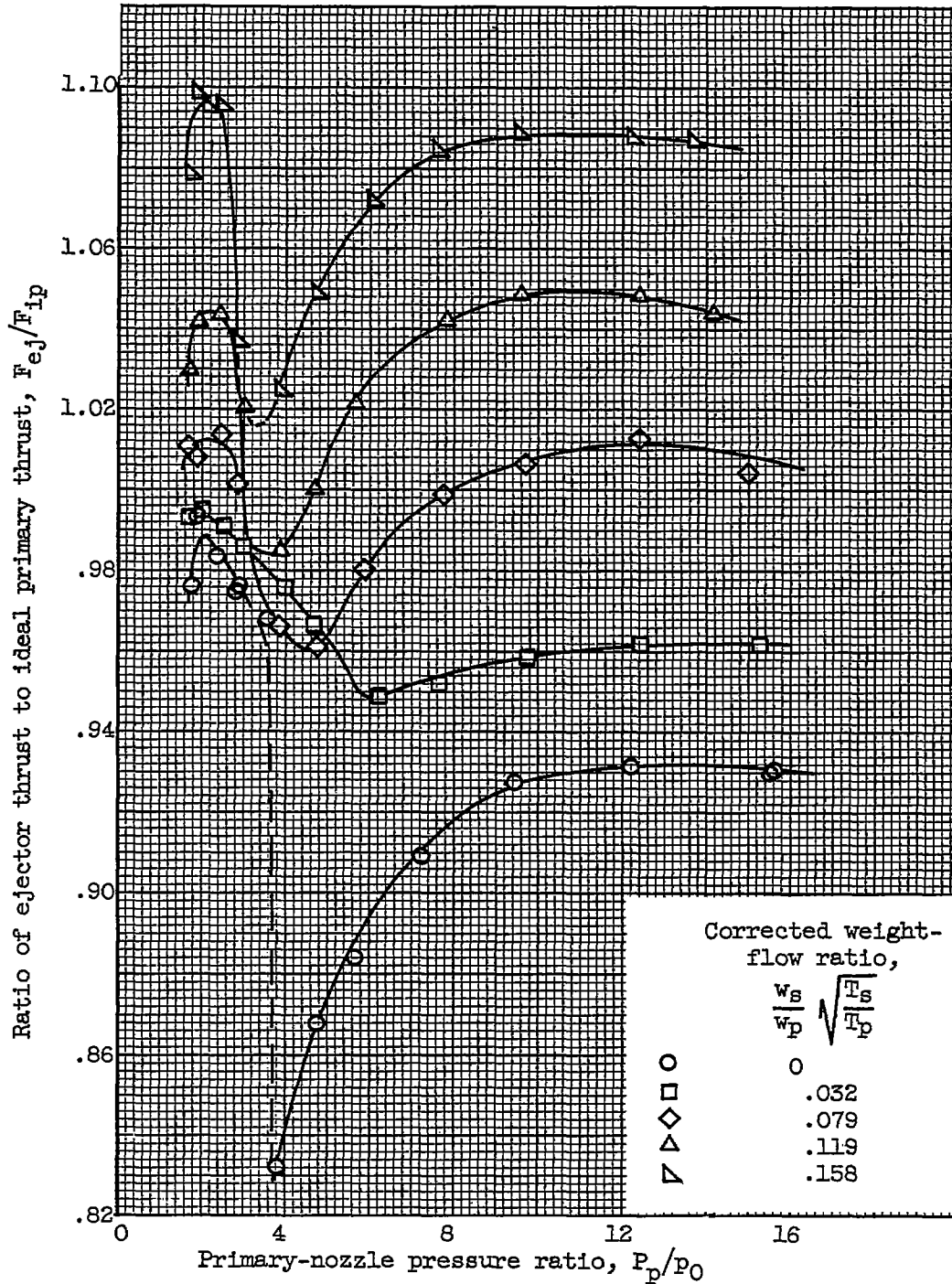
Figure 8. - Continued. Performance of ejector 4. Exit diameter ratio, 1.46; throat diameter ratio, 1.10; spacing ratio, 0.69; flow divergence angle, 19°; shroud divergence angle, 15°.



(b) Concluded. Flow characteristics.

Figure 8. - Concluded. Performance of ejector 4. Exit diameter ratio, 1.46; throat diameter ratio, 1.10; spacing ratio, 0.69; flow divergence angle, 19° ; shroud divergence angle, 15° .

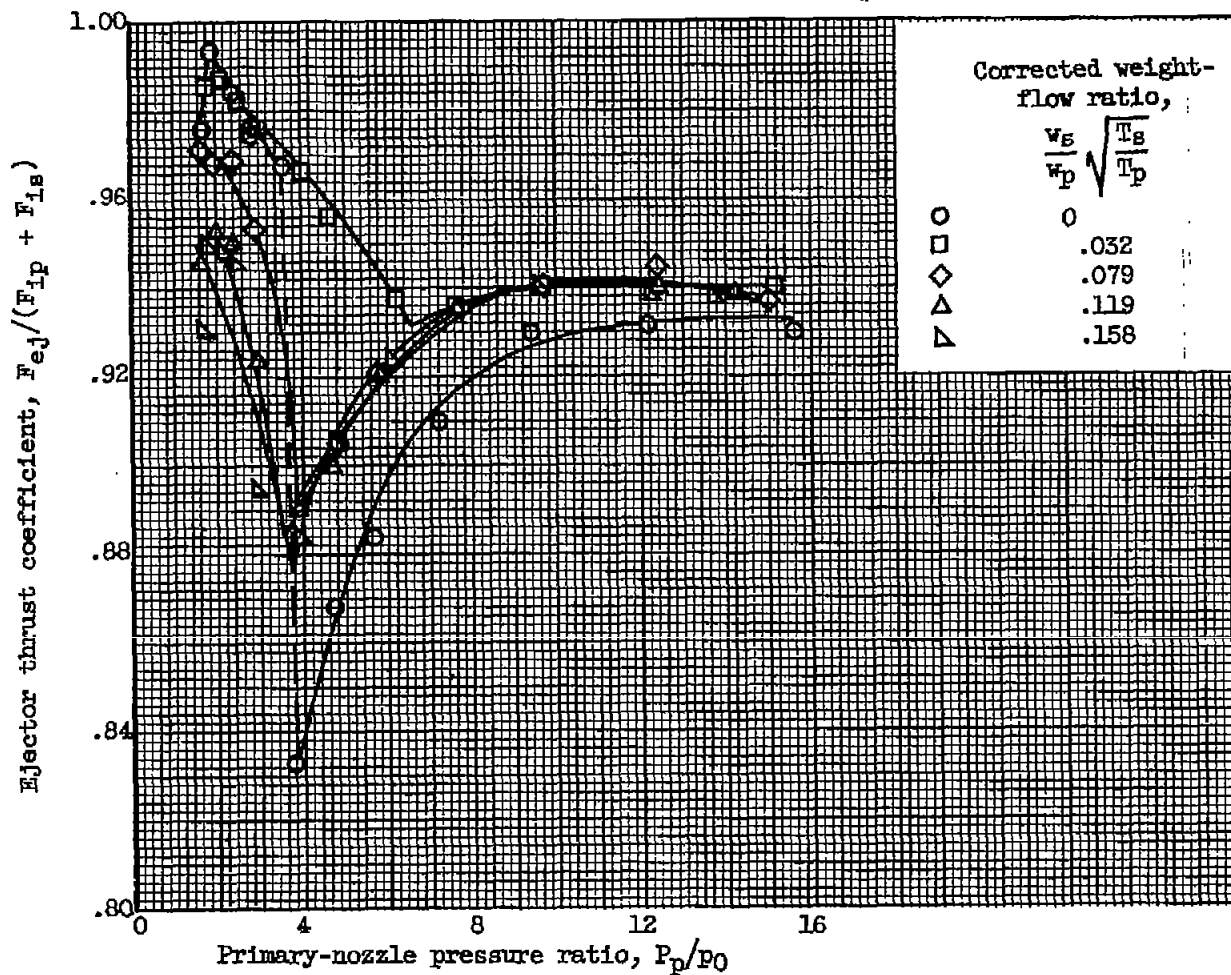
4400



(a) Thrust characteristics.

Figure 9. - Performance of ejector 5. Exit diameter ratio, 1.46; throat diameter ratio, 1.10; spacing ratio, 0.51; flow divergence angle, 25°; shroud divergence angle, 20°.

~~CONFIDENTIAL~~

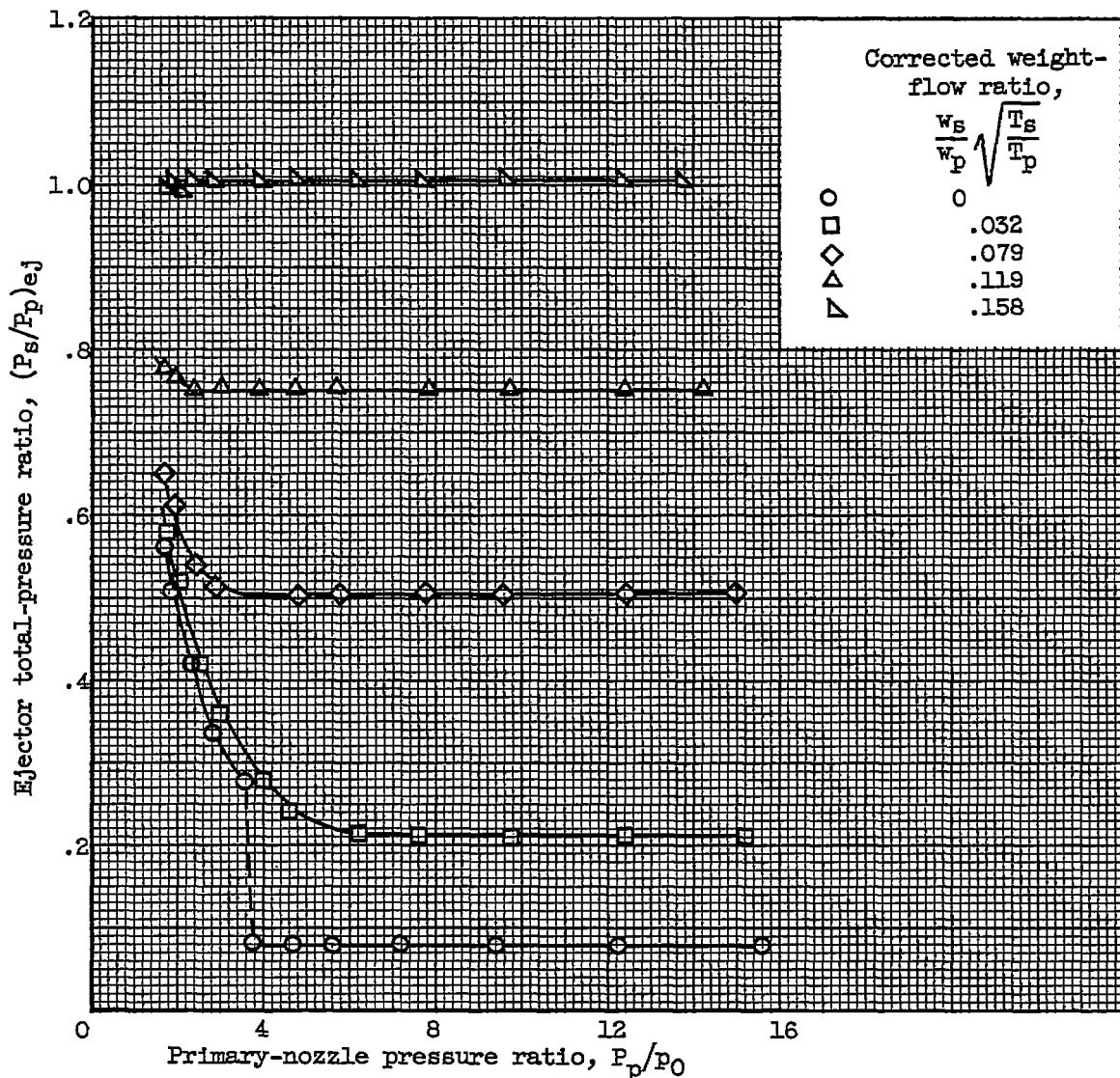


(a) Concluded. Thrust characteristics.

Figure 9. - Continued. Performance of ejector 5. Exit diameter ratio, 1.46; throat diameter ratio, 1.10; spacing ratio, 0.51; flow divergence angle, 25° ; shroud divergence angle, 20° .

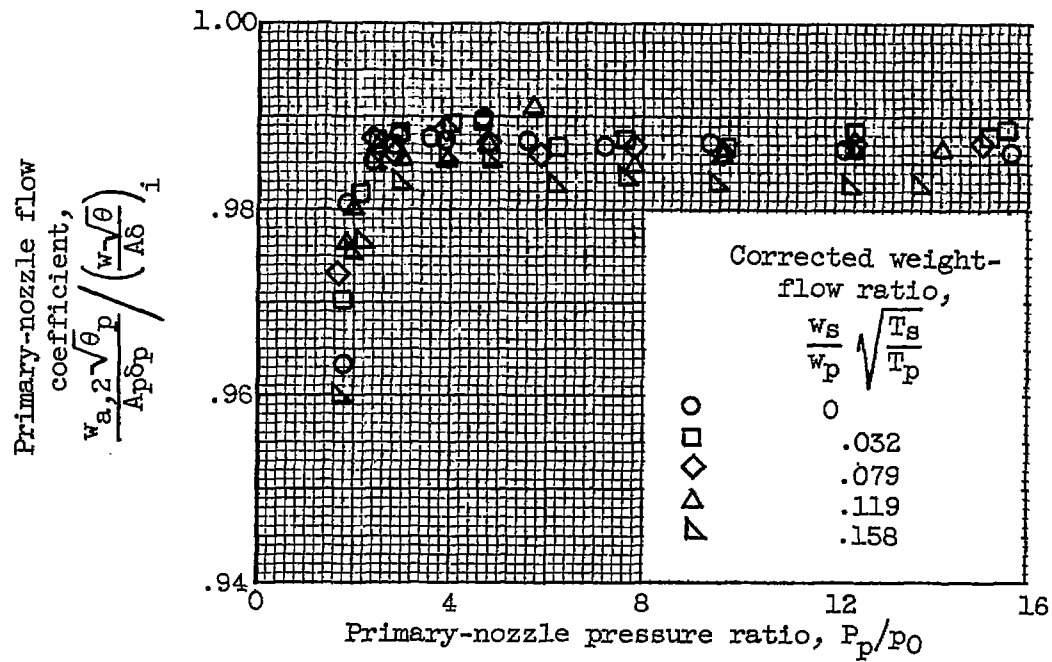
4400

CP-6



(b) Flow characteristics.

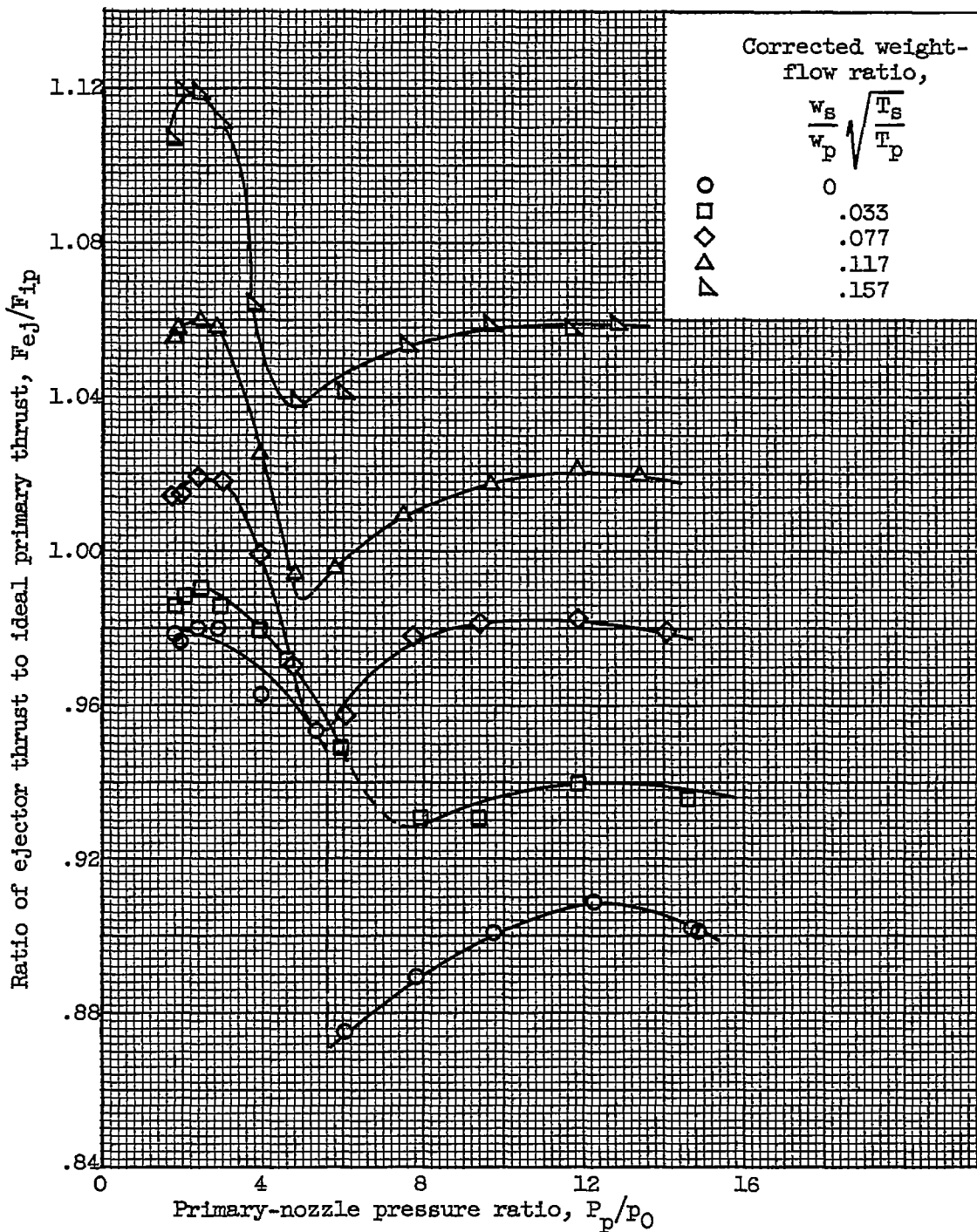
Figure 9. - Continued. Performance of ejector 5. Exit diameter ratio, 1.46; throat diameter ratio, 1.10; spacing ratio, 0.51; flow divergence angle, 25°; shroud divergence angle, 20°.



(b) Concluded. Flow characteristics.

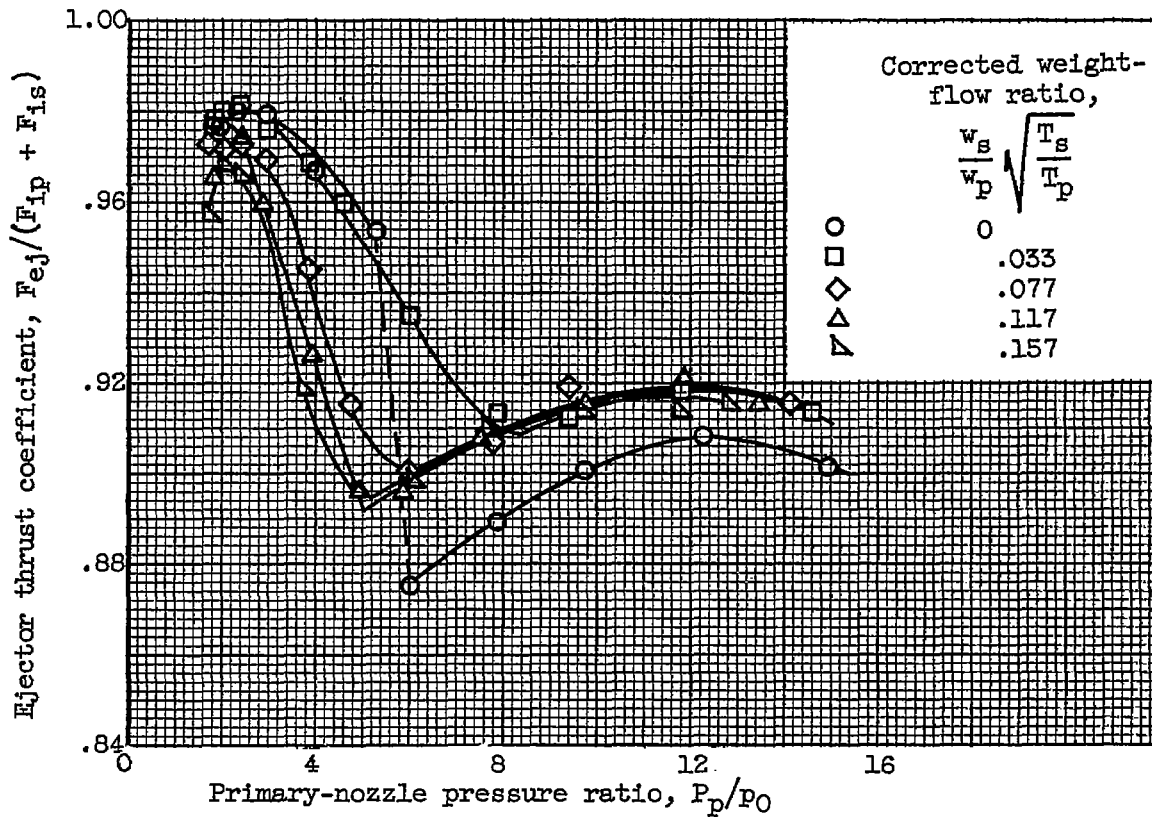
Figure 9. - Concluded. Performance of ejector 5.
Exit diameter ratio, 1.46; throat diameter ratio, 1.10; spacing ratio, 0.51; flow divergence angle, 25°; shroud divergence angle, 20°.

4400
CP-6 back



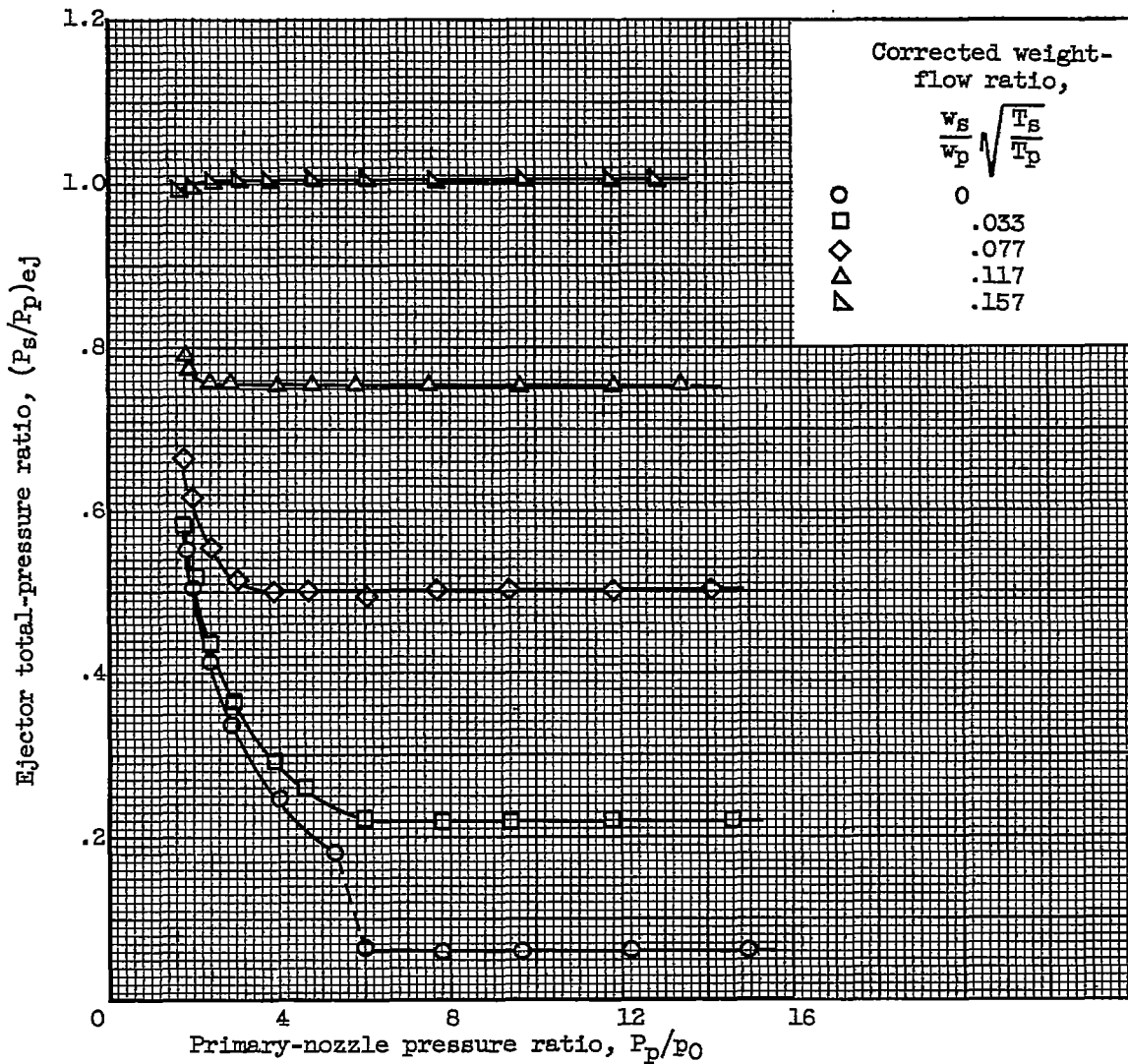
(a) Thrust characteristics.

Figure 10. - Performance of ejector 6. Exit diameter ratio, 1.46; throat diameter ratio, 1.10; spacing ratio, 0.40; flow divergence angle, 30°; shroud divergence angle, 25°.



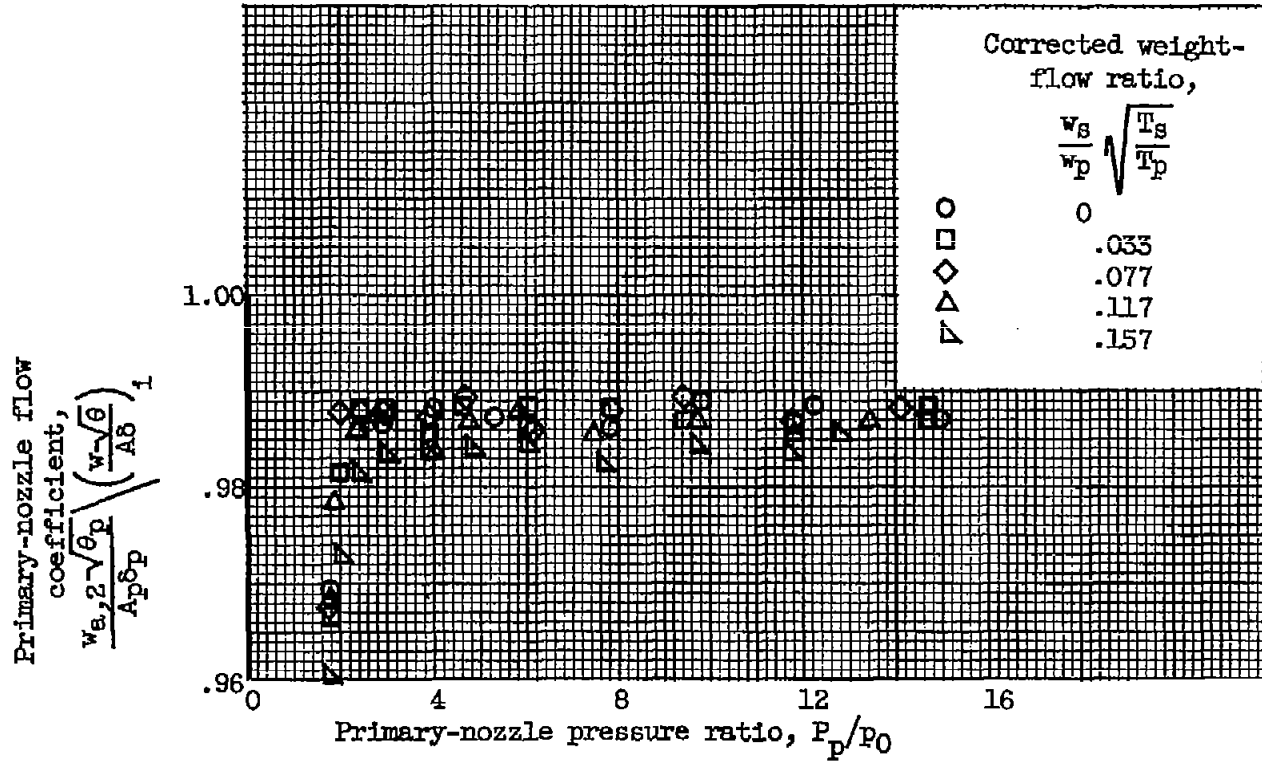
(a) Concluded. Thrust characteristics.

Figure 10. - Continued. Performance of ejector 6. Exit diameter ratio, 1.46; throat diameter ratio, 1.10; spacing ratio, 0.40; flow divergence angle, 30° ; shroud divergence angle, 25° .



(b) Flow characteristics.

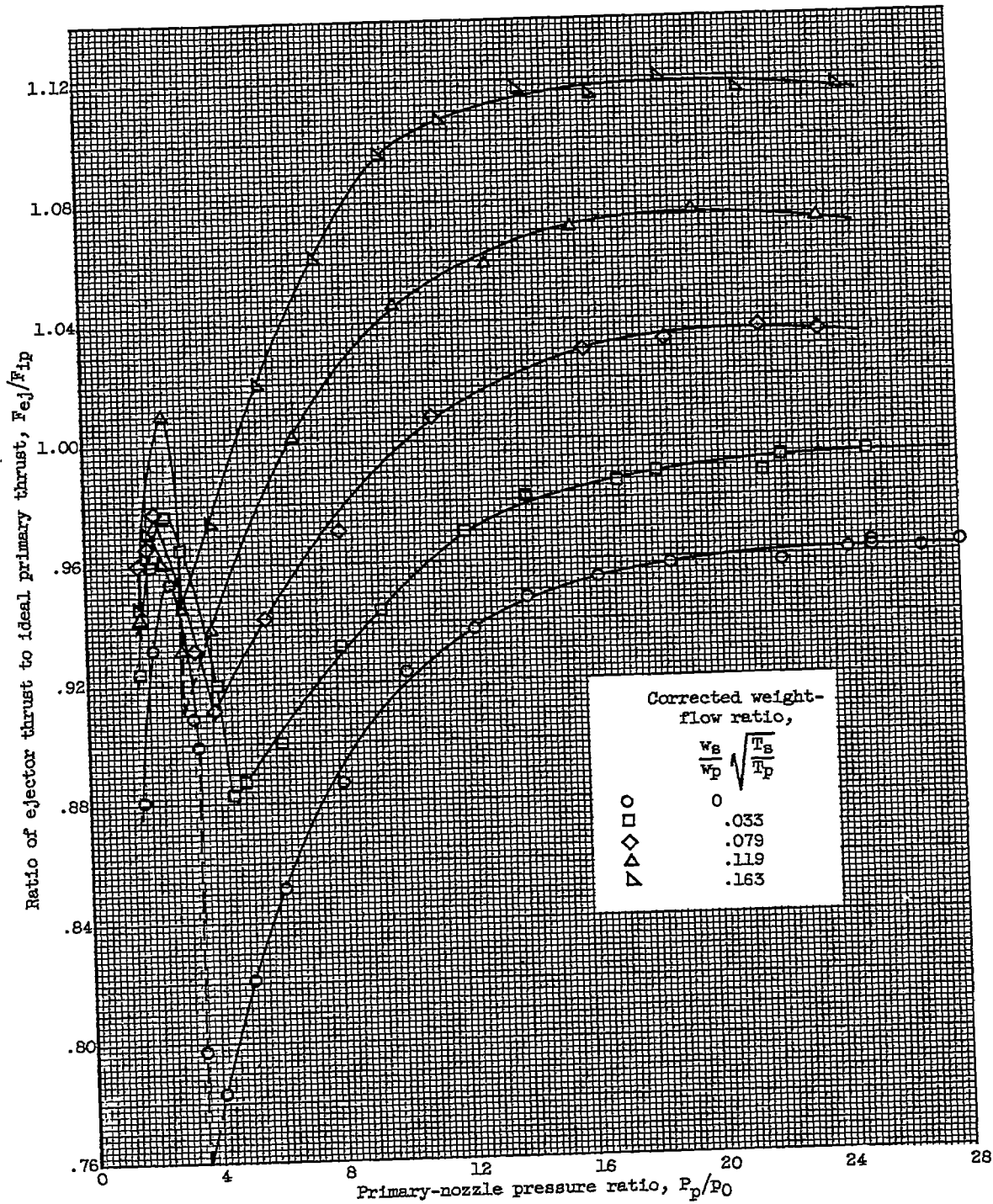
Figure 10. - Continued. Performance of ejector 6. Exit diameter ratio, 1.46; throat diameter ratio, 1.10; spacing ratio, 0.40; flow divergence angle, 30° ; shroud divergence angle, 25° .



(b) Concluded. Flow characteristics.

Figure 10. - Concluded. Performance of ejector 6. Exit diameter ratio, 1.46; throat diameter ratio, 1.10; spacing ratio, 0.40; flow divergence angle, 30° ; shroud divergence angle, 25° .

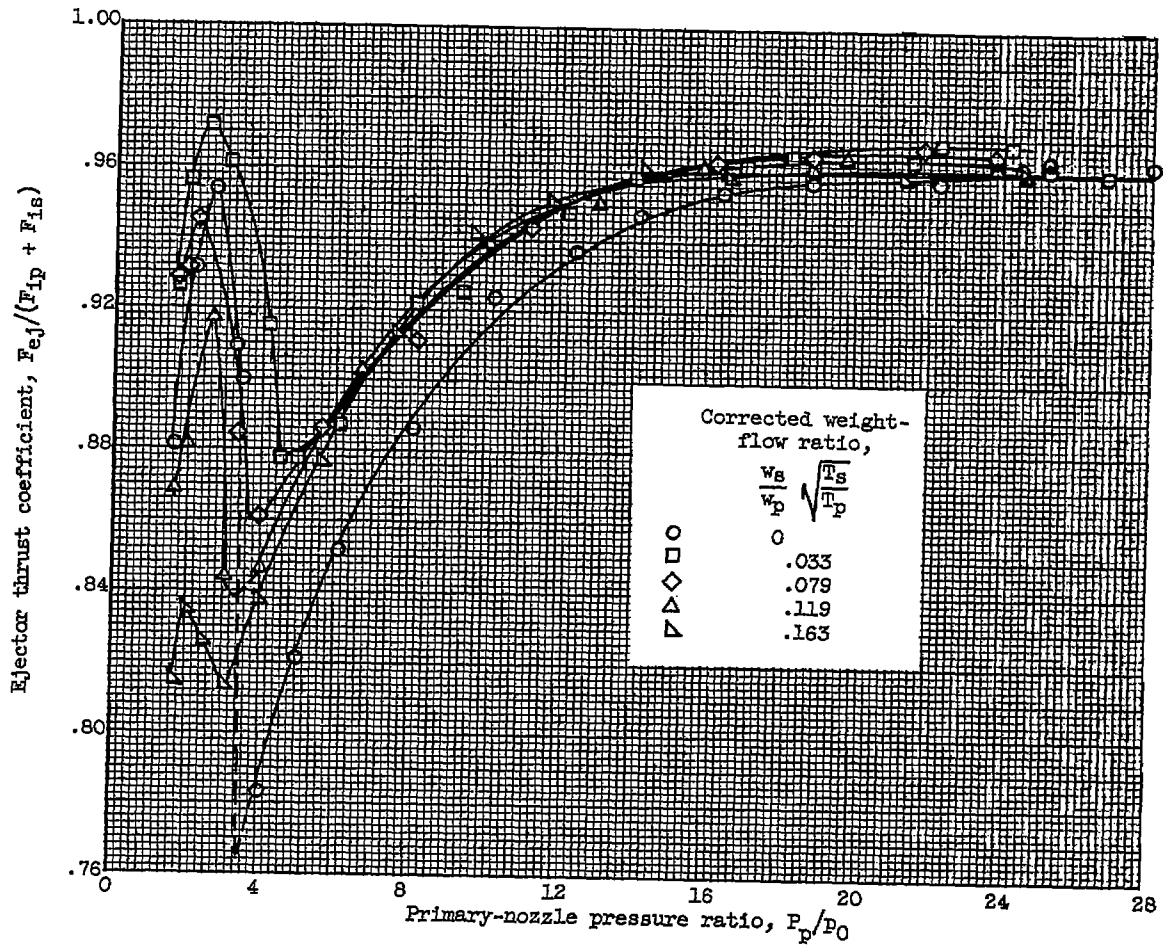
4400



(a) Thrust characteristics.

Figure 11. - Performance of ejector 7. Exit diameter ratio, 1.82; throat diameter ratio, 1.10; spacing ratio, 1.31; flow divergence angle, 17°; shroud divergence angle, 15°.

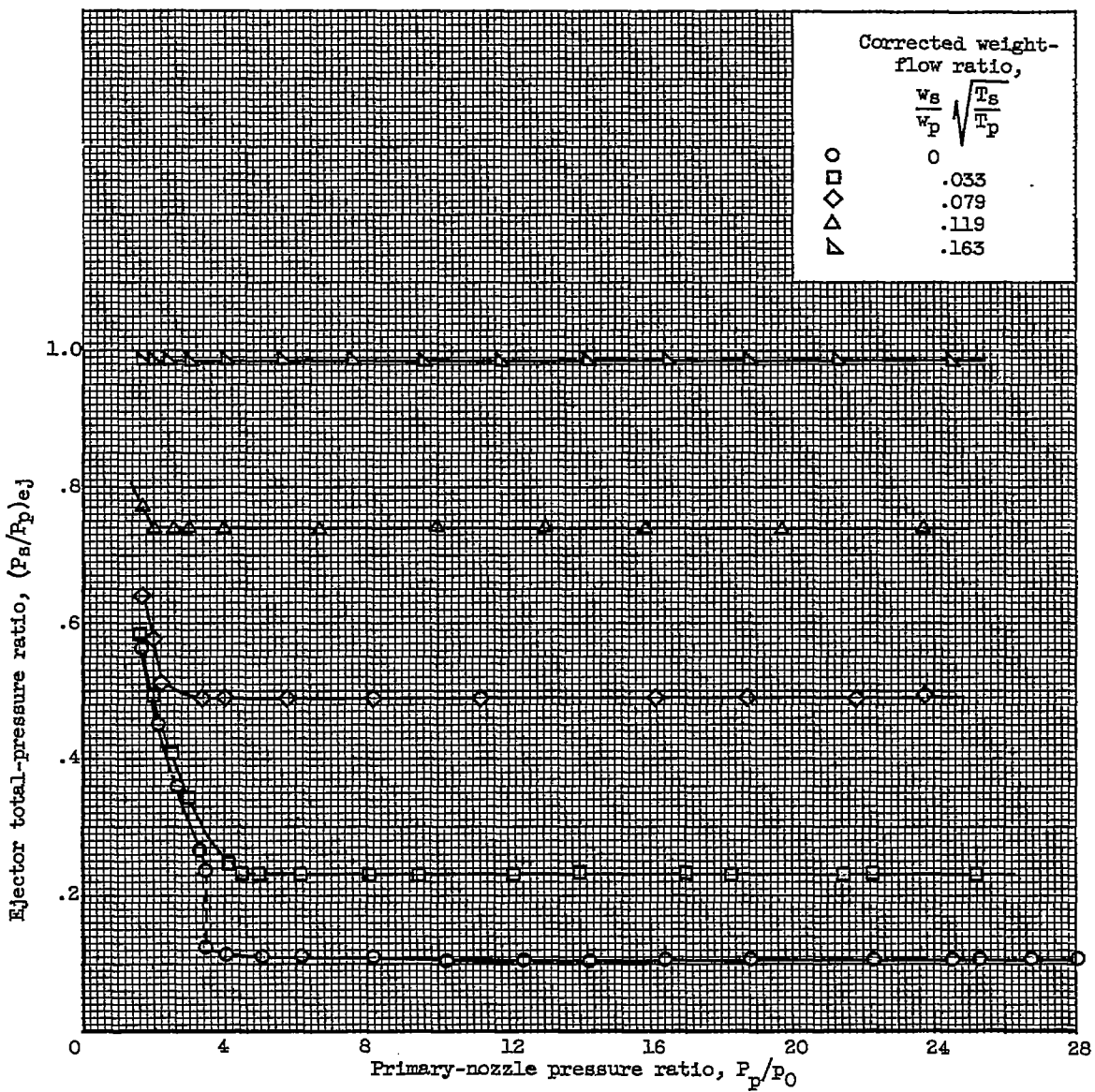
~~CONFIDENTIAL~~



(a) Concluded. Thrust characteristics.

Figure 11. - Continued. Performance of ejector 7. Exit diameter ratio, 1.82; throat diameter ratio, 1.10; spacing ratio, 1.31; flow divergence angle, 17°; shroud divergence angle, 15°.

CF-7 4400

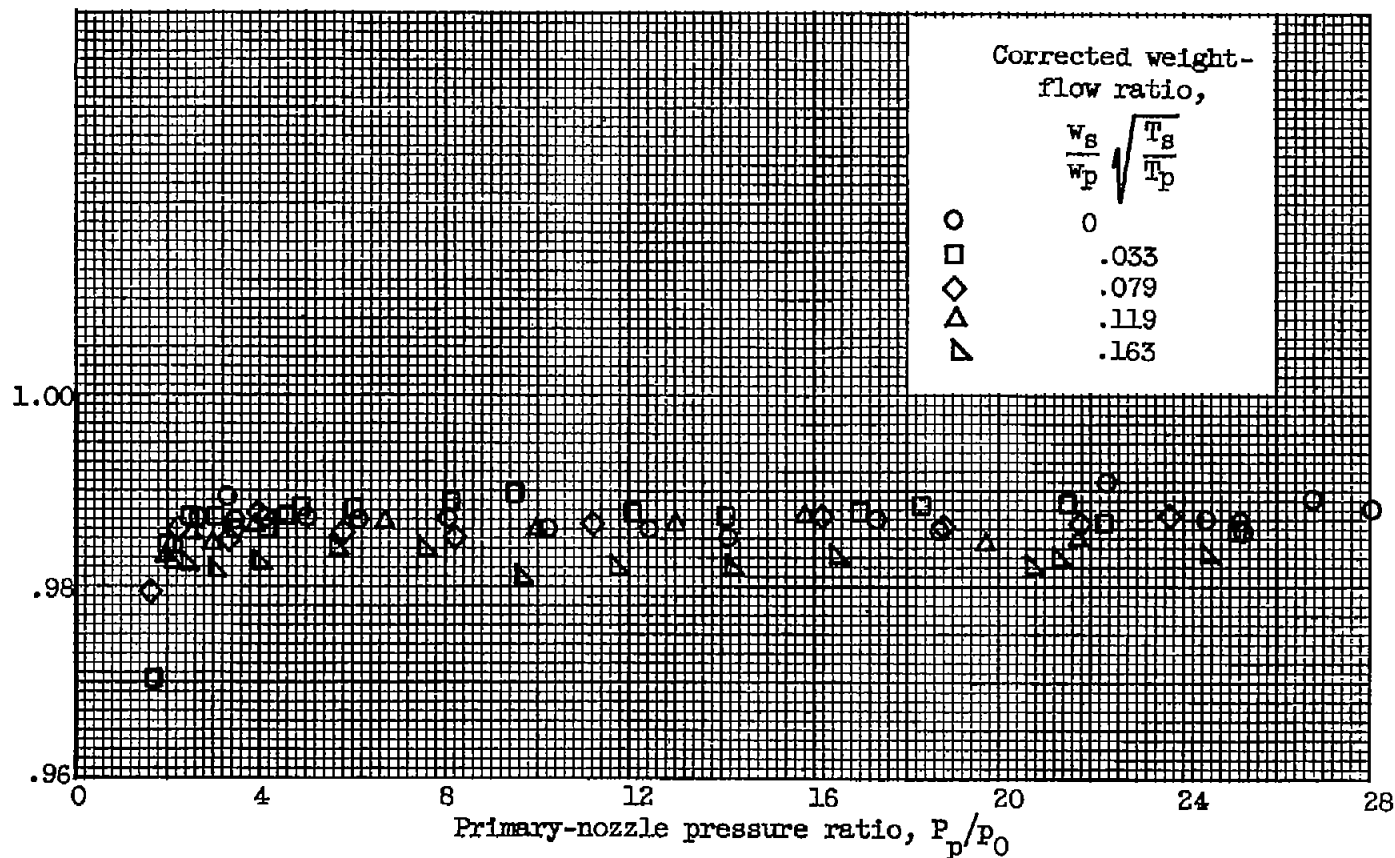


(b) Flow characteristics.

Figure 11. - Continued. Performance of ejector 7. Exit diameter ratio, 1.82; throat diameter ratio, 1.10; spacing ratio, 1.31; flow divergence angle, 17°, shroud divergence angle, 15°.

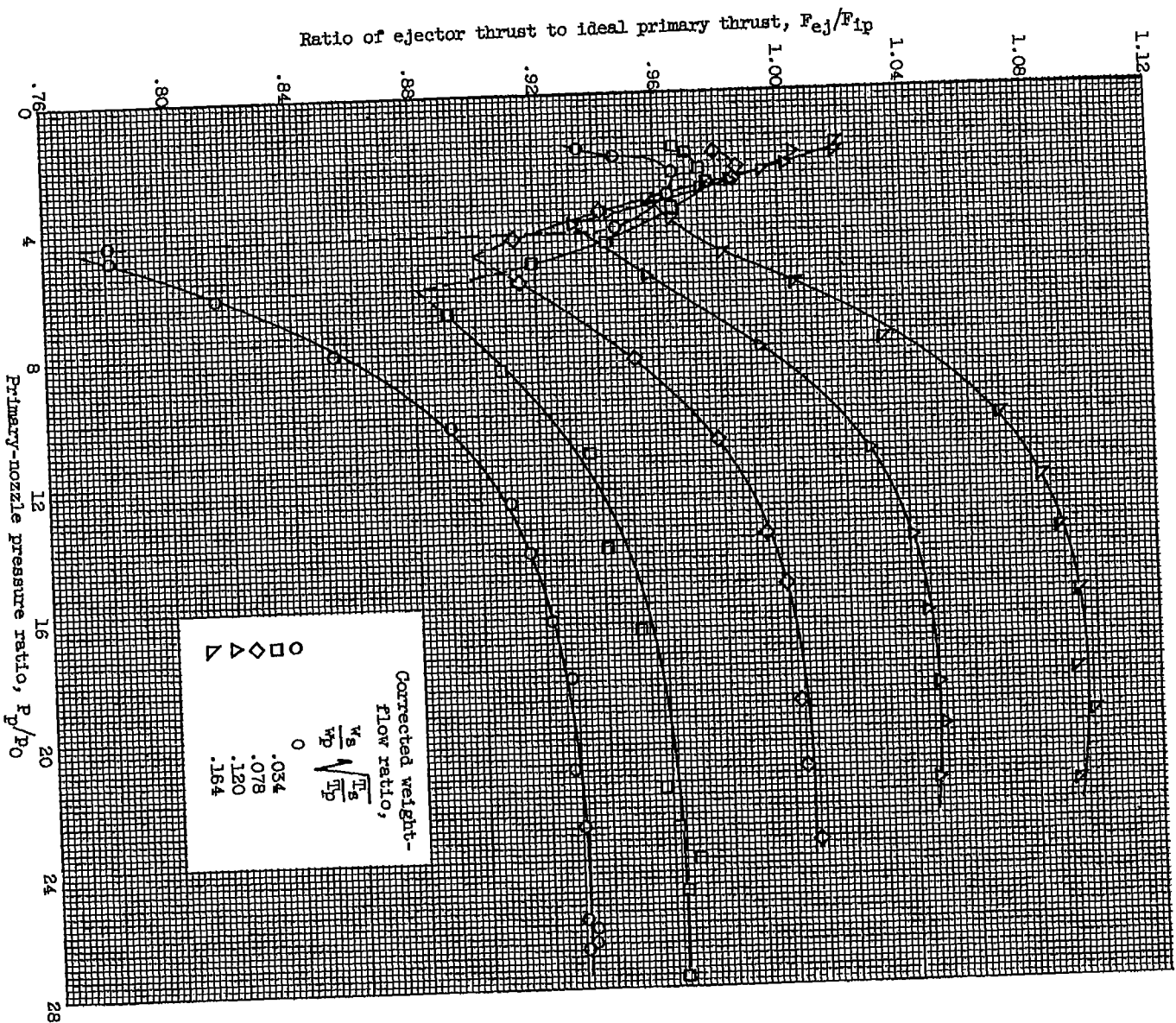
Primary-nozzle flow

$$\text{coefficient, } \frac{w_s \sqrt{\theta_p}}{A_p \delta p} \left(\frac{w \sqrt{\theta}}{A \delta} \right)_1$$



(b) Concluded. Flow characteristics.

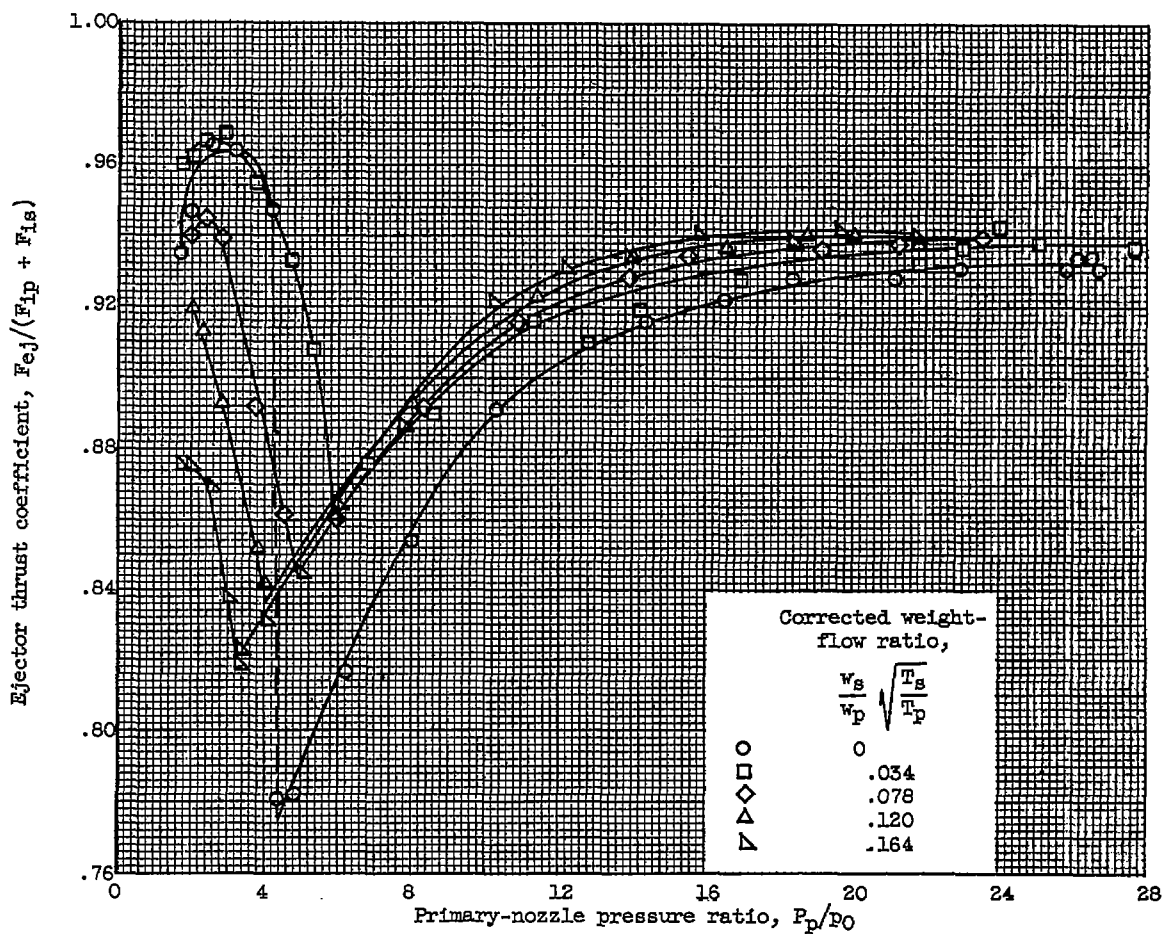
Figure 11. - Concluded. Performance of ejector 7. Exit diameter ratio, 1.82; throat diameter ratio, 1.10; spacing ratio, 1.31; flow divergence angle, 17°; shroud divergence angle, 15°.



(a) Thrust characteristics.

Figure 12. - Performance of ejector 8. Exit diameter ratio, 1.81; throat diameter ratio, 1.10; spacing ratio, 0.98; flow divergence angle, 25°; shroud divergence angle, 20°.

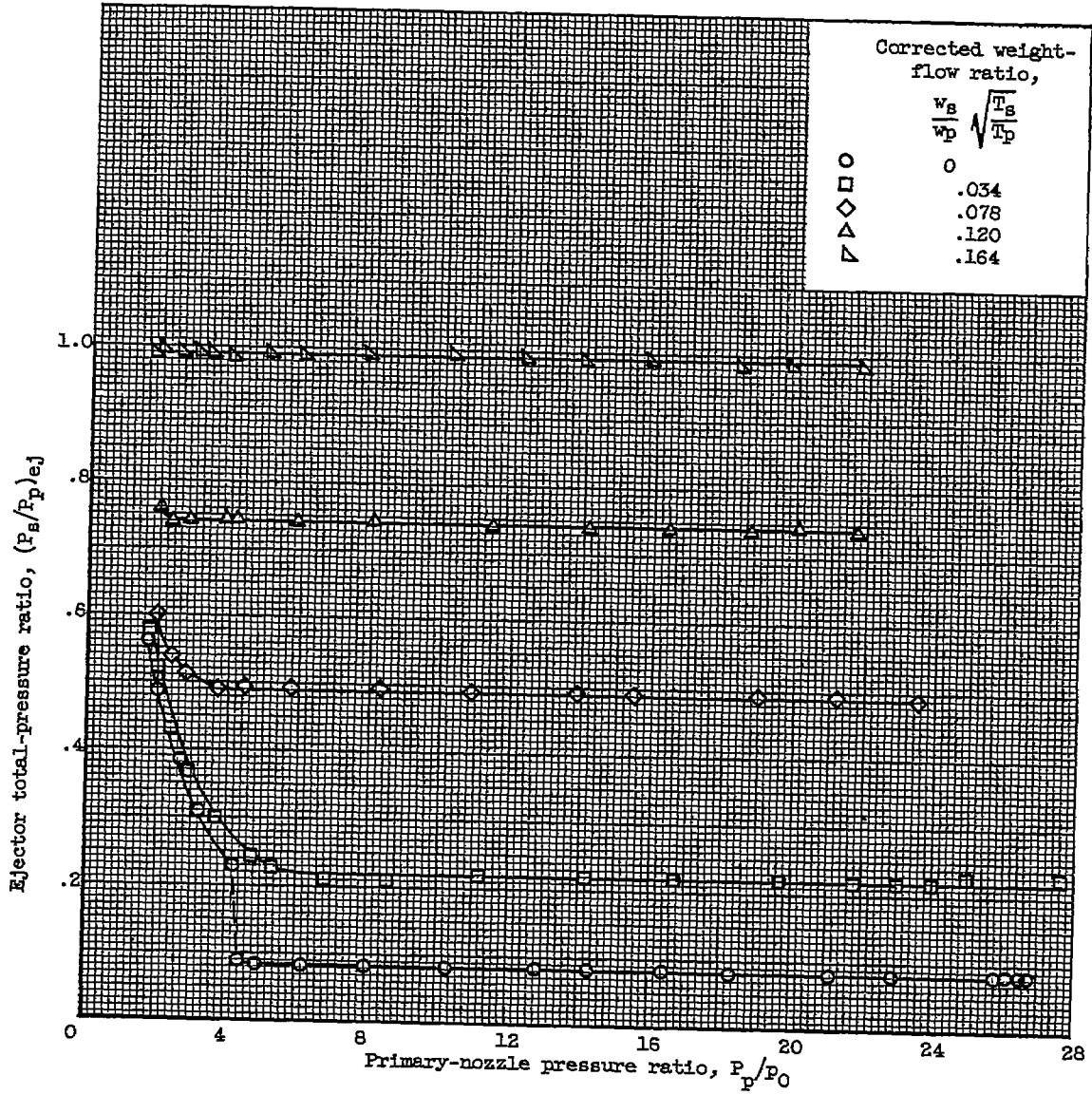
SECRET



(a) Concluded. Thrust characteristics.

Figure 12. - Continued. Performance of ejector 8. Exit diameter ratio, 1.81; throat diameter ratio, 1.10; spacing ratio, 0.98; flow divergence angle, 25° ; shroud divergence angle, 20° .

4400

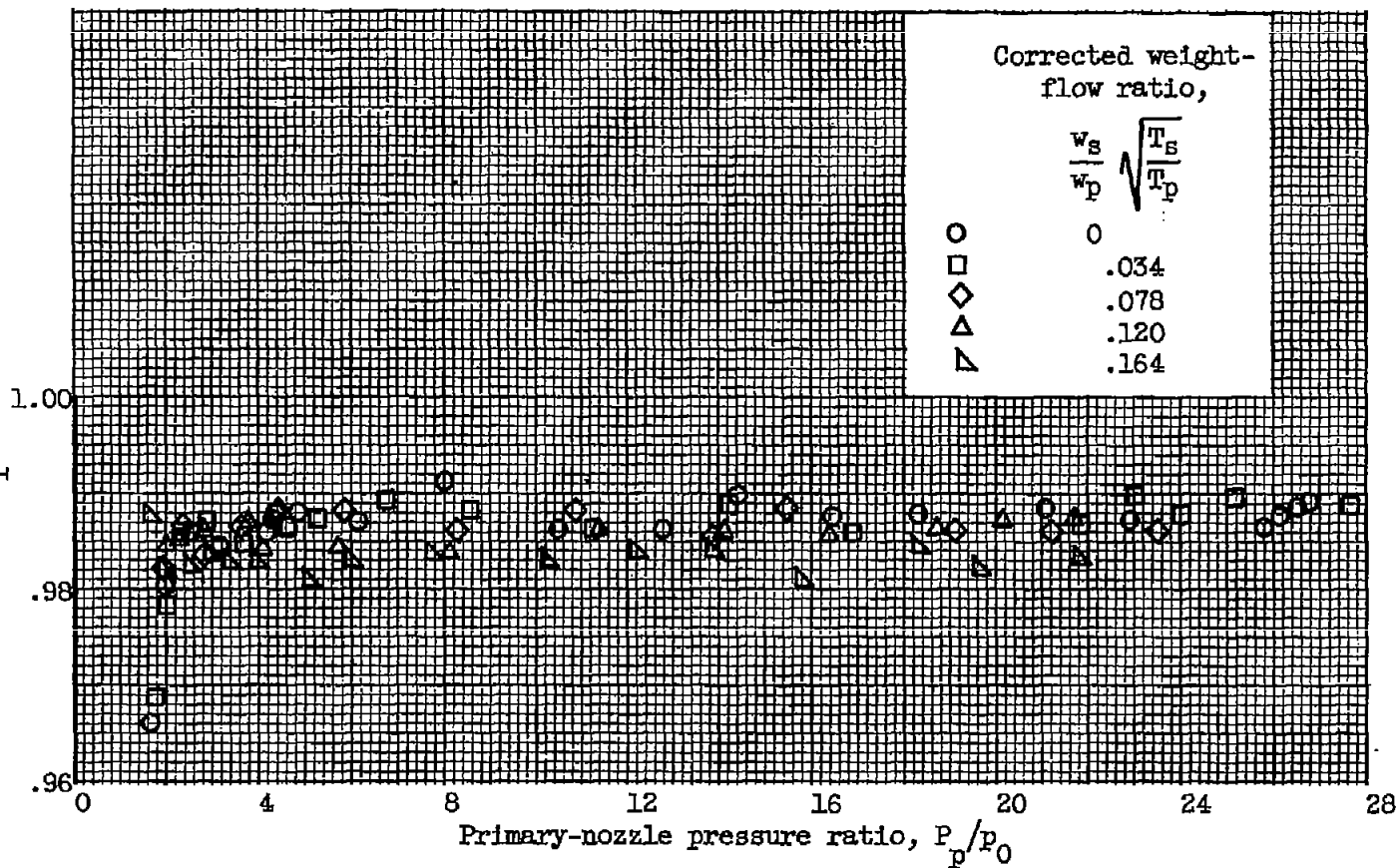


(b) Flow characteristics.

Figure 12. - Continued. Performance of ejector 8. Exit diameter ratio, 1.81; throat diameter ratio, 1.10; spacing ratio, 0.98; flow divergence angle, 23°; shroud divergence angle, 20°.

Primary-nozzle flow

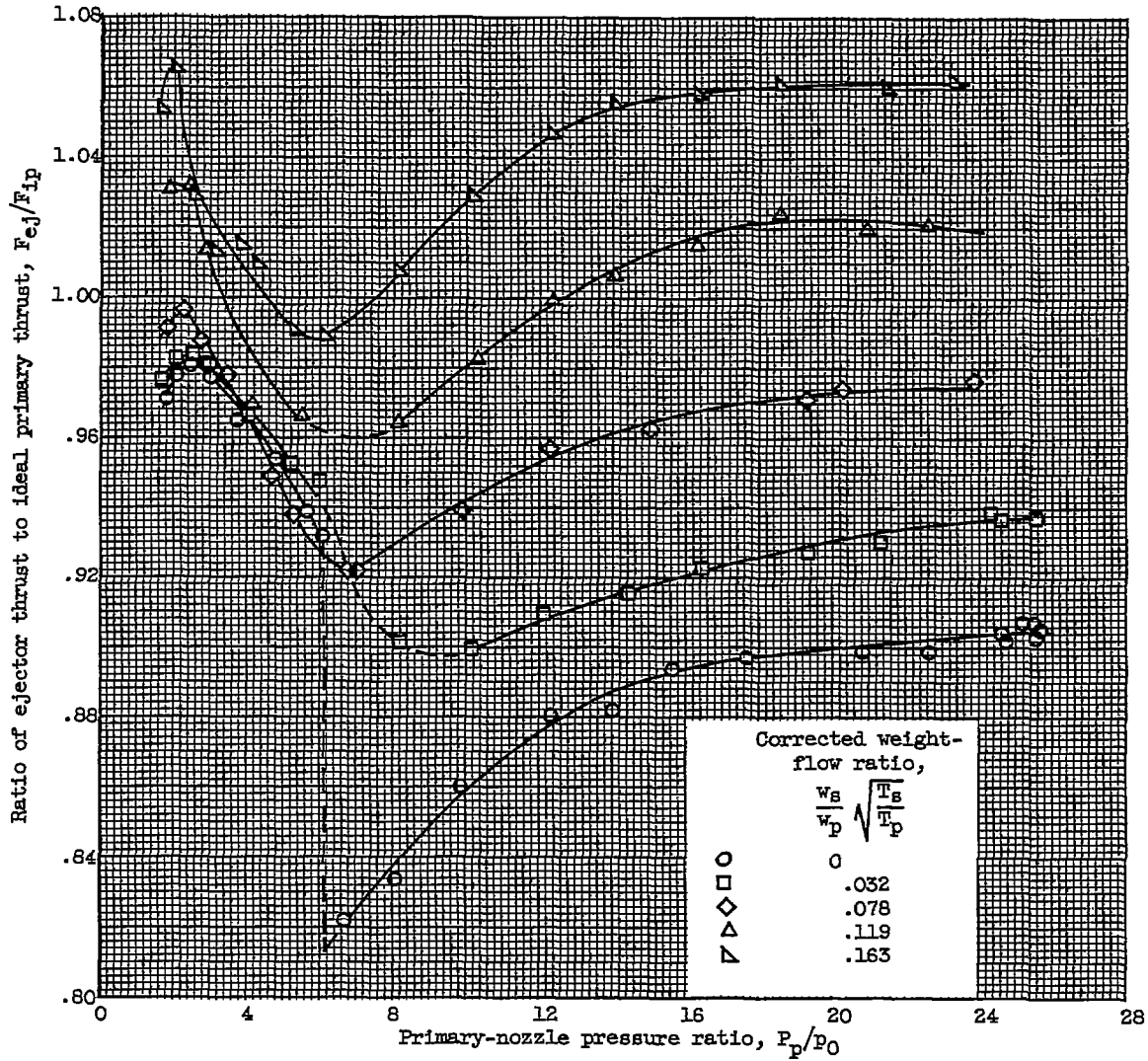
$$\text{coefficient, } \frac{w_a \sqrt{\theta}}{A_p \delta p} \left(\frac{w \sqrt{\theta}}{A_B} \right)_1$$



(b) Concluded. Flow characteristics.

Figure 12. - Concluded. Performance of ejector 8. Exit diameter ratio, 1.81; throat diameter ratio, 1.10; spacing ratio, 0.98; flow divergence angle, 23°; shroud divergence angle, 20°.

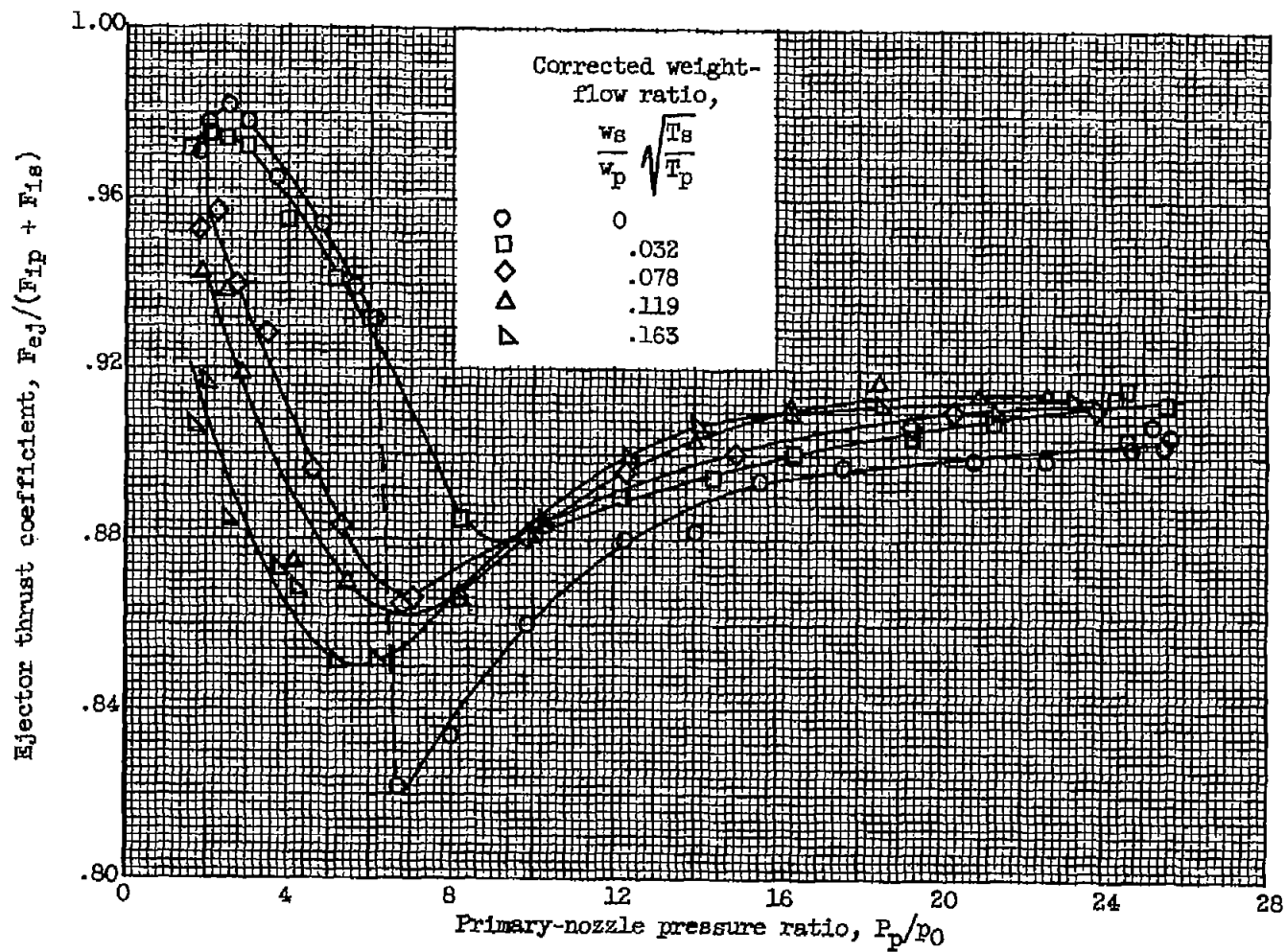
4400



(a) Thrust characteristics.

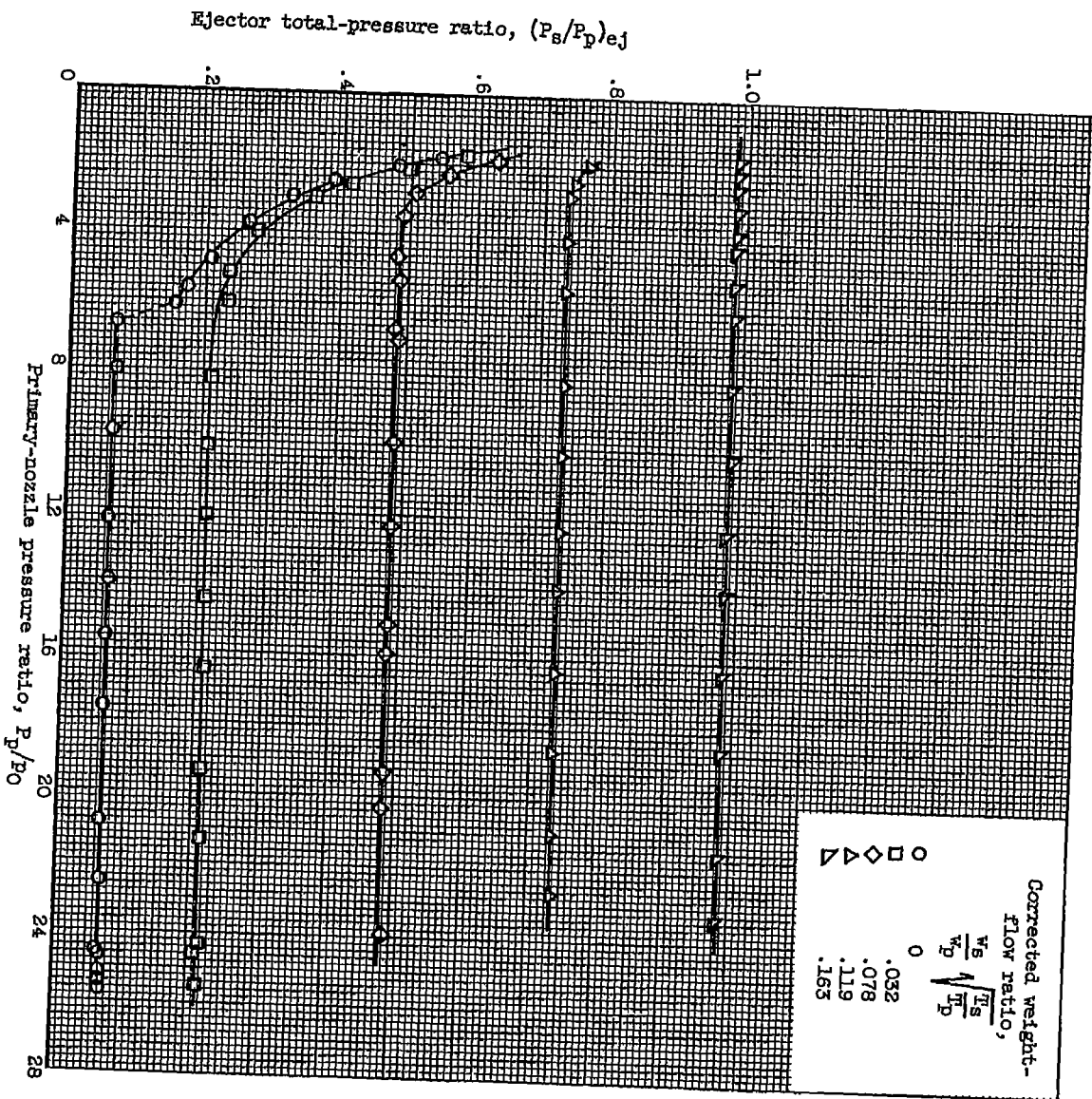
Figure 13. - Performance of ejector 9. Exit diameter ratio, 1.81; throat diameter ratio, 1.10; spacing ratio, 0.76; flow divergence angle, 28° ; shroud divergence angle, 25° .

CONFIDENTIAL



(a) Concluded. Thrust characteristics.

Figure 13. - Continued. Performance of ejector 9. Exit diameter ratio, 1.81; throat diameter ratio, 1.10; spacing ratio, 0.76; flow divergence angle, 28° ; shroud divergence angle, 25° .



(b) Flow characteristics.

Figure 15. - Continued. Performance of ejector 9. Exit diameter ratio, 1.81; throat diameter ratio, 1.10; spacing ratio, 0.76; flow divergence angle, 28°; shroud divergence angle, 25°.

NOT REPRODUCIBLE

Ejector thrust
coefficient
at design
pressure ratio,
 $F_{ej}/(F_{ip} + F_{is})$

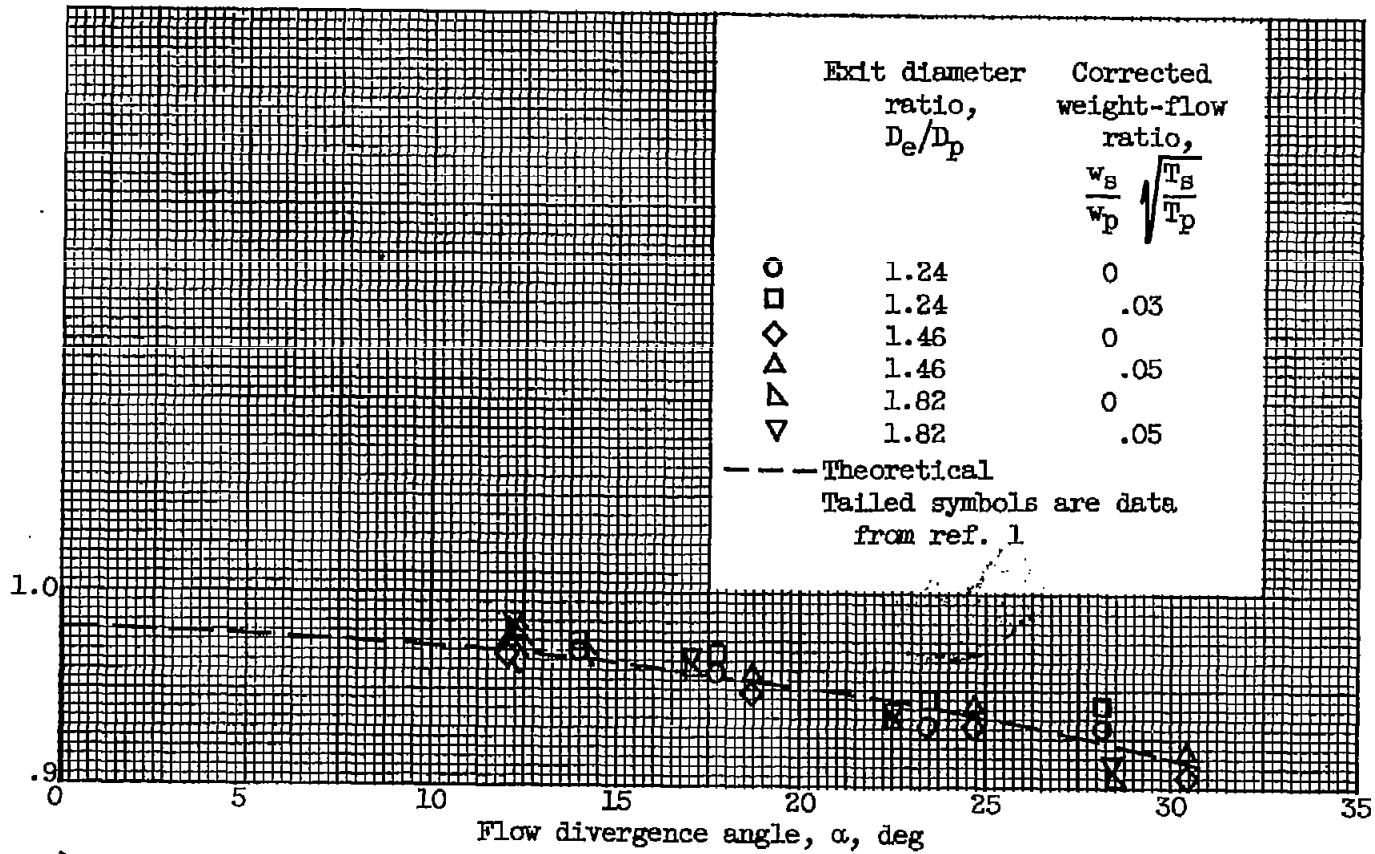


Figure 14. - Effect of flow divergence angle on thrust coefficient at design pressure ratio.

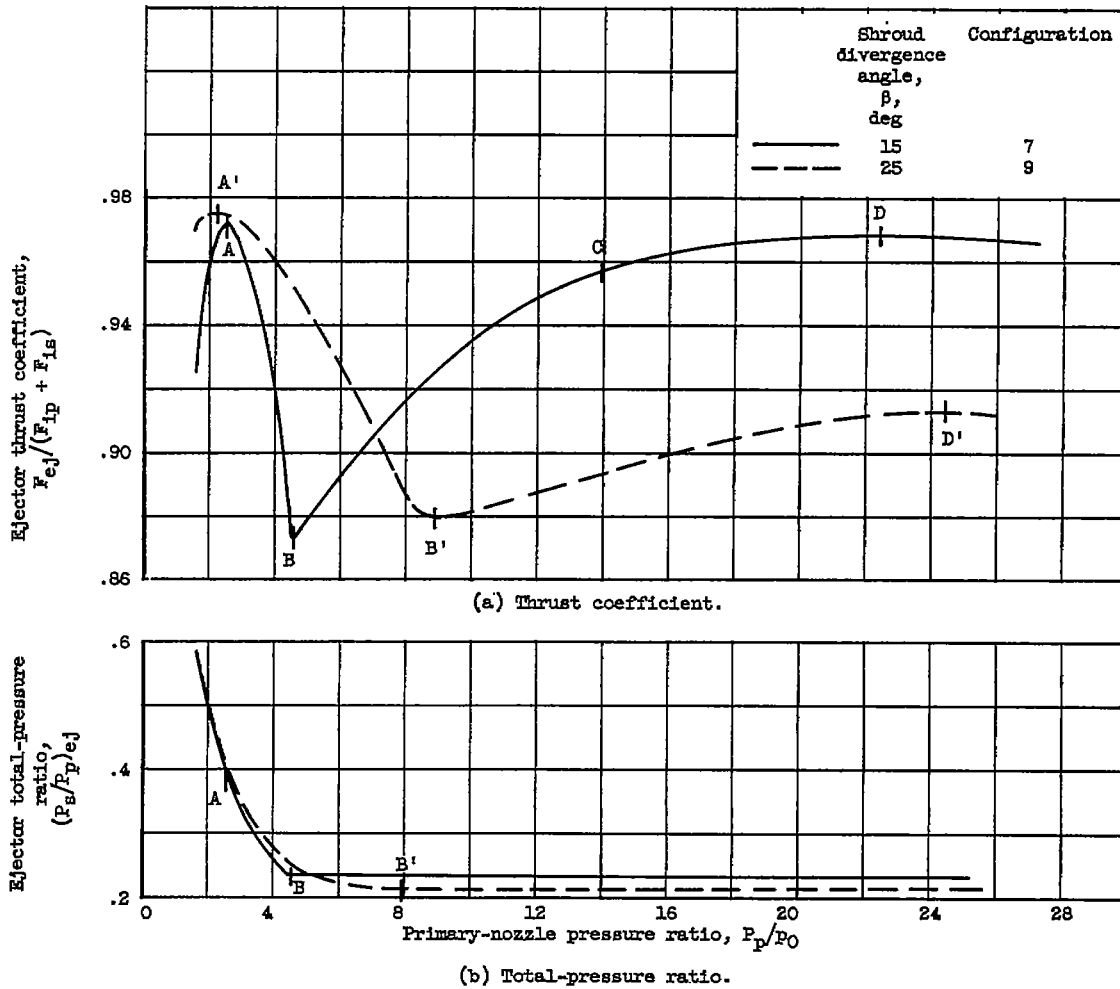
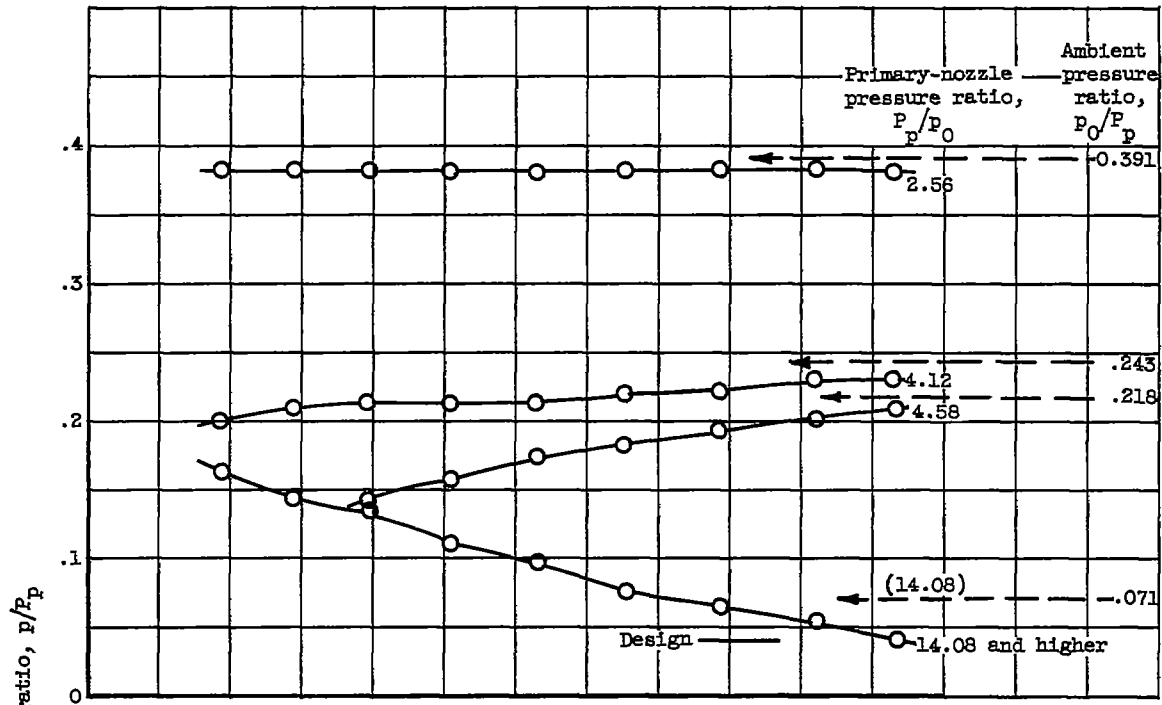
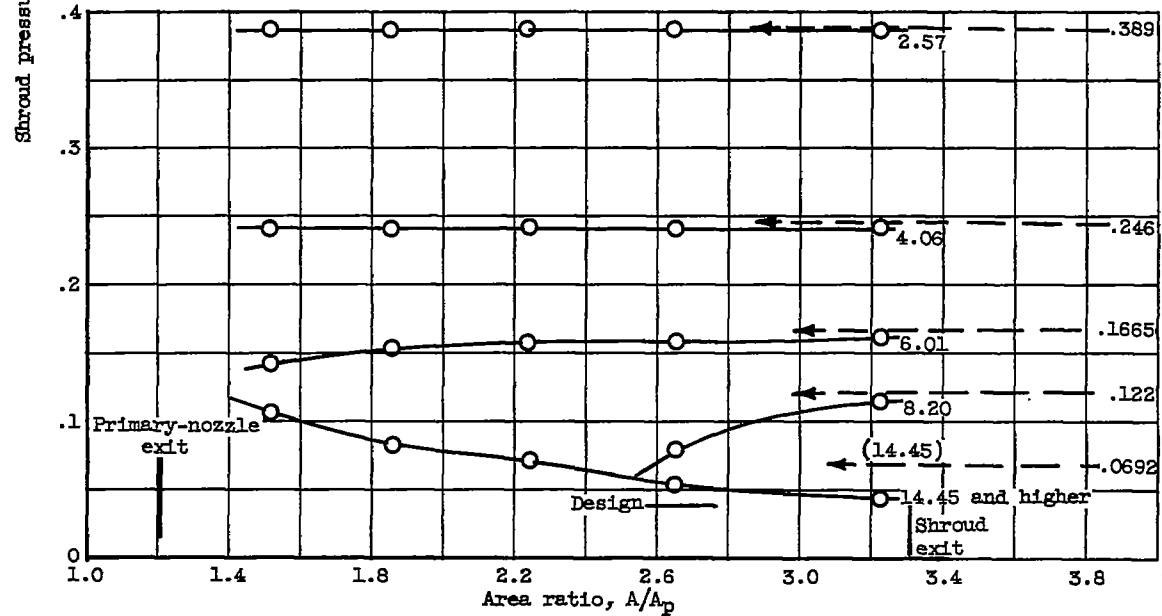


Figure 15. - Performance of configurations 7 and 9 at weight-flow ratio of about 0.032. Exit diameter ratio, 1.8; throat diameter ratio, 1.10.

4400

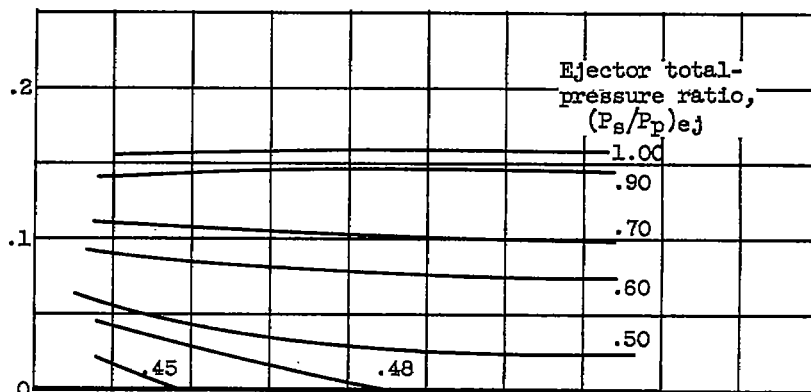


(a) Configuration 7; shroud divergence angle, 15° ; corrected weight-flow ratio, 0.032.

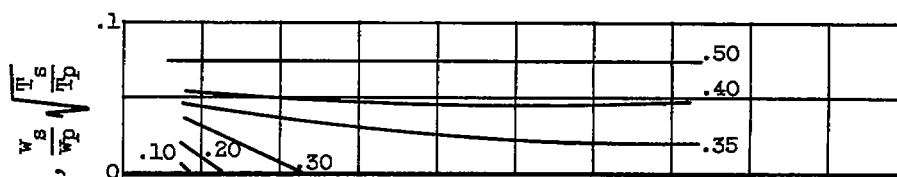


(b) Configuration 9; shroud divergence angle, 25° ; corrected weight-flow ratio, 0.033.

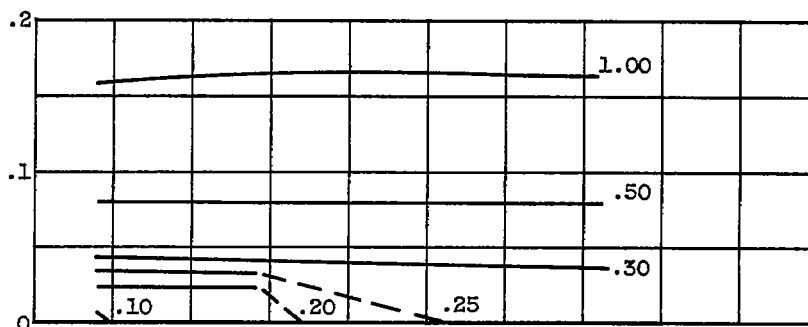
Figure 16. - Shroud static-pressure distribution for configurations 7 and 9 for various primary-nozzle pressure ratios.

~~CONFIDENTIAL~~

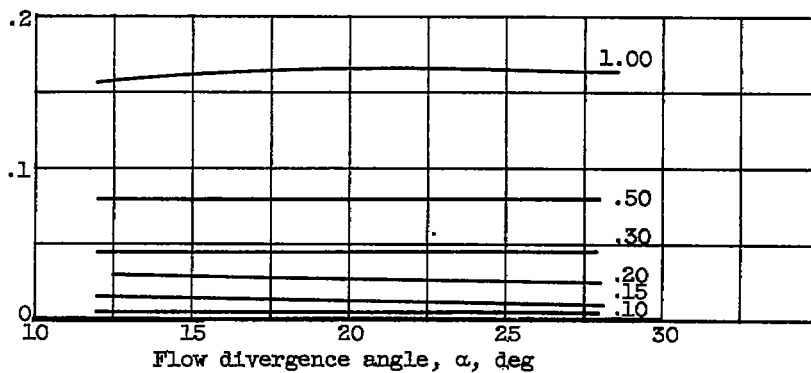
(a) Primary-nozzle pressure ratio, 2.



(b) Primary-nozzle pressure ratio, 3.



(c) Primary-nozzle pressure ratio, 4.

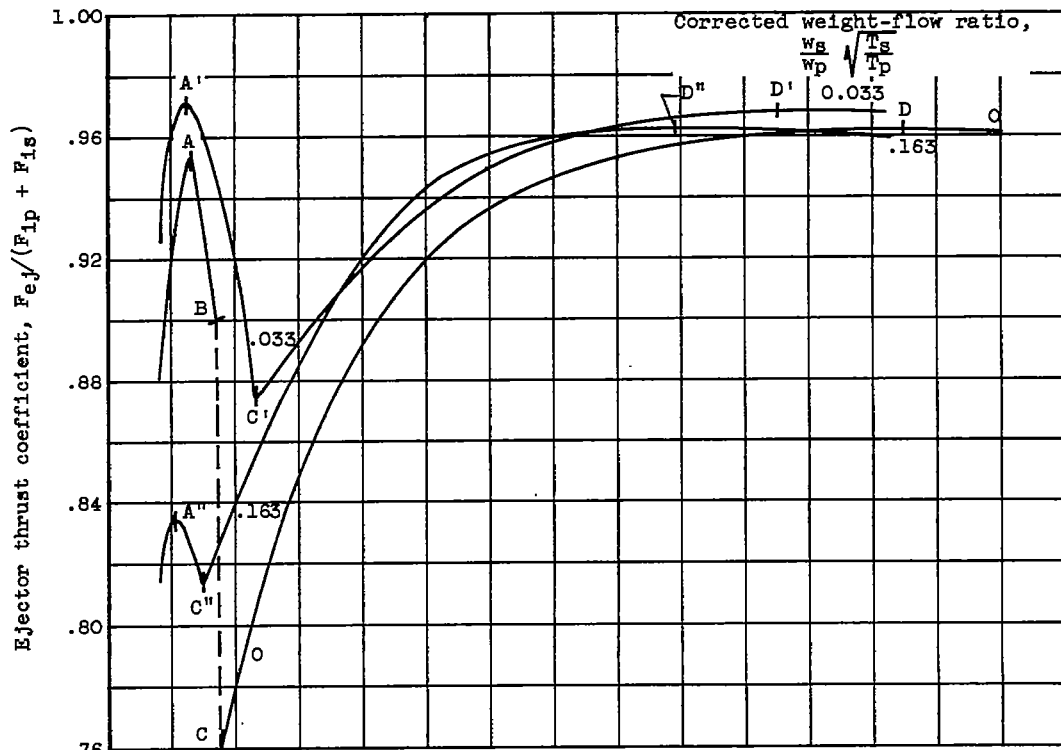


(d) Primary-nozzle pressure ratio, 6 and above.

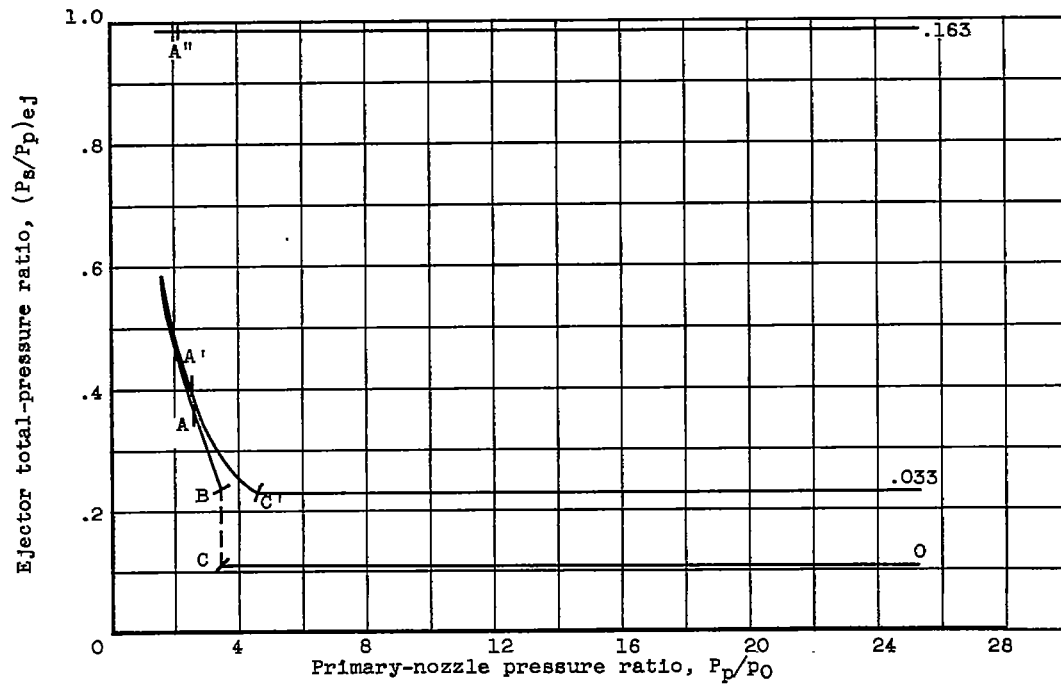
Figure 17. - Variation of corrected weight-flow ratio with flow divergence angle. (Data from configuration 10 of ref. 1 and configurations 7 to 9.)

~~CONFIDENTIAL~~

4400



(a) Thrust coefficient.



(b) Total-pressure ratio.

Figure 18. - Performance of configuration 7 for several weight-flow ratios.

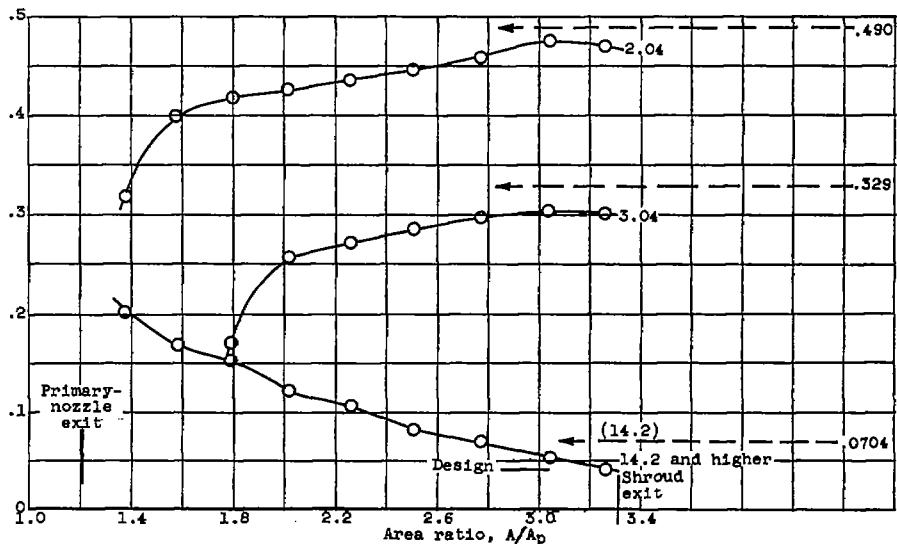
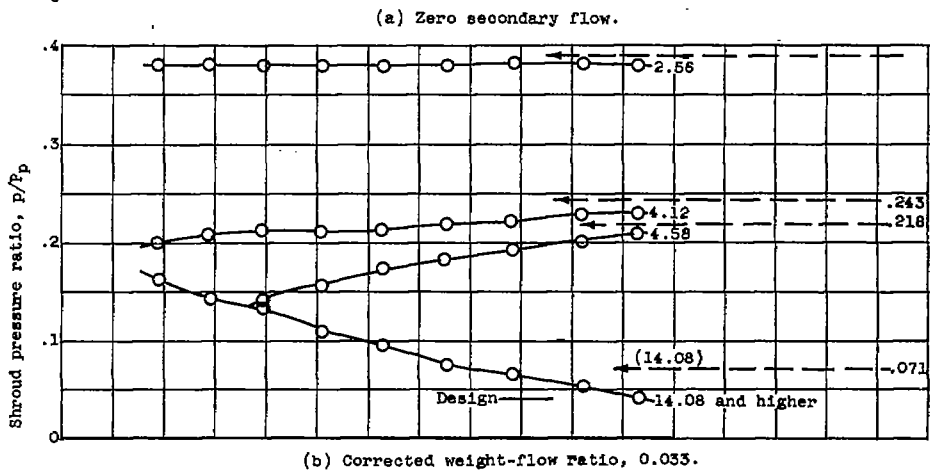
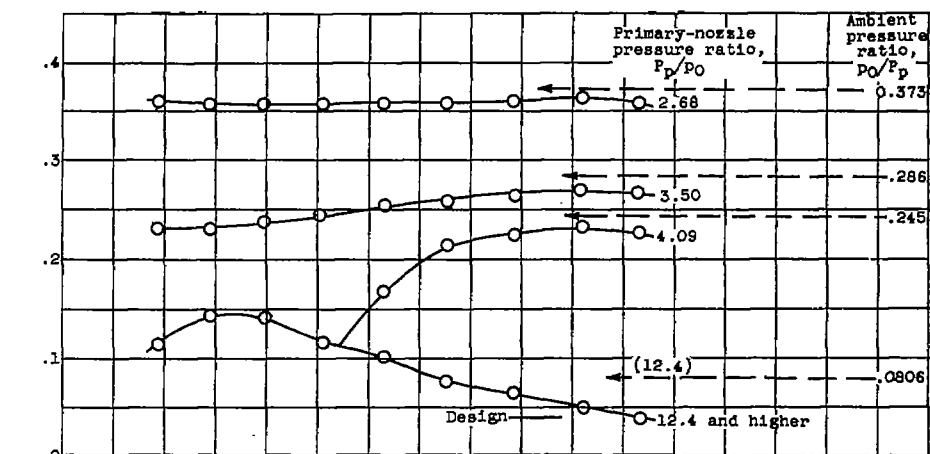
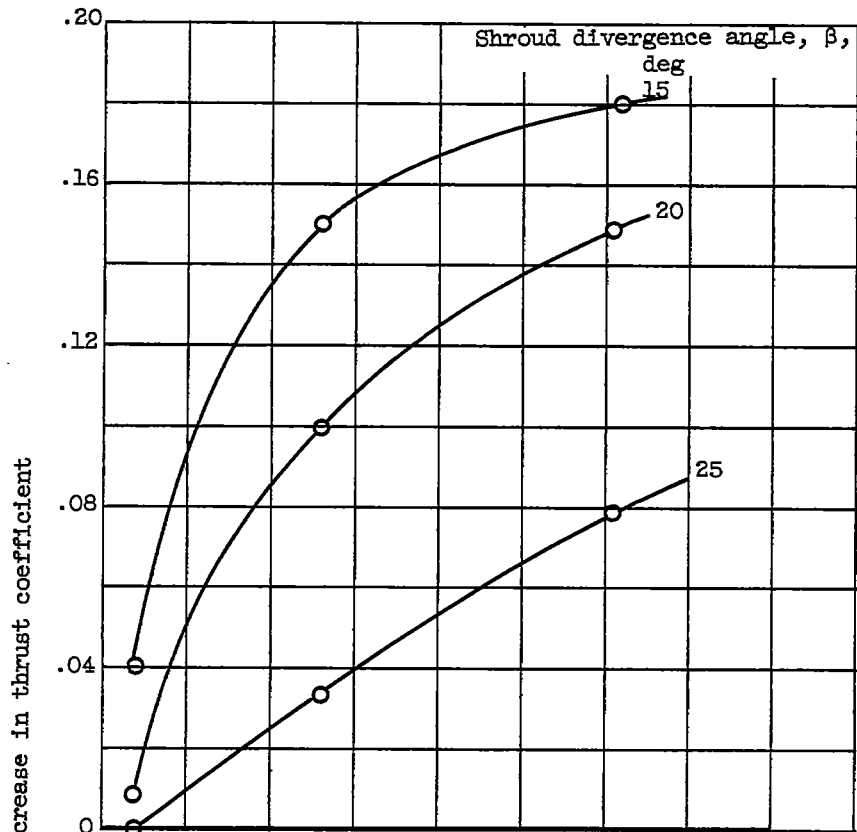
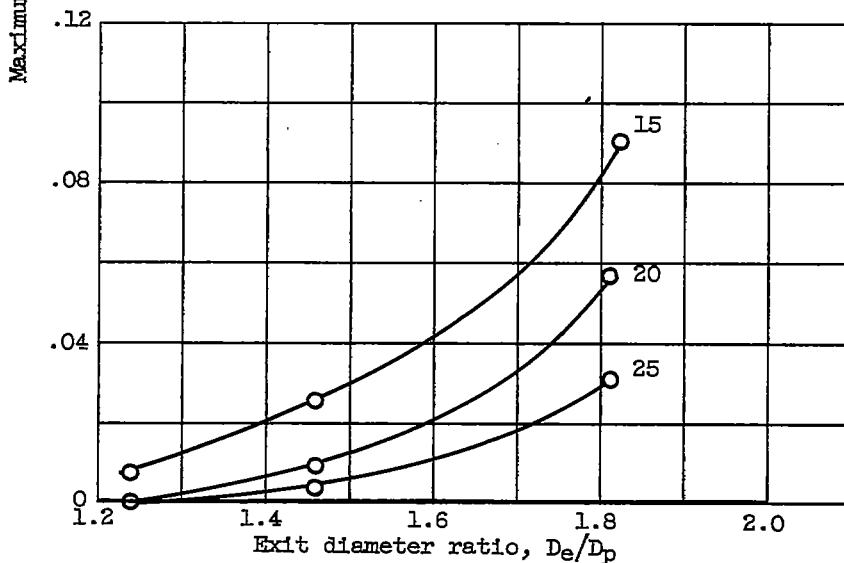


Figure 19. - Shroud static-pressure distribution for configuration 7 at several corrected weight-flow ratios.



(a) Zero secondary flow.



(b) Corrected weight-flow ratio, 0.03.

Figure 20. - Effect of secondary airflow on thrust coefficient at off-design (overexpanded) conditions.

